Analysis of ubiquitin signaling and membrane traffic regulation in plant C/N-nutrient responses

植物の C/N 栄養応答における

ユビキチンシグナルと膜交通制御の解析

Yoko Hasegawa

A Dissertation
Submitted to the Graduate School of Life Science, Hokkaido University
in partial fulfillment of the Requirements for the Degree of
Doctor of Philosophy in Life Science

Biosystems Science Course
Graduate School of Life Science
Hokkaido University, Sapporo, Japan

March, 2022

TABLES OF CONTENTS

SUMMARY IN JAPANESE

Analysis of ubiquitin signaling and membrane traffic regulation

in plant C/N-nutrient responses

（植物の C/N 栄養応答におけるユビキチンシグナルと膜交通制御の解析）

ユビキチン化は，ユビキチンという 76 アミノ酸残基から成る小さなタンパク質の付加による, 可逆的な翻訳後修飾の一種である。ユビキチン化は, 当初 “ATP を利用するエネルギー依存的なタンパク質の分解機構” として発見されたが, 後に分解のみならず，様々なシグナルとして機能することが明らかとなった。ユビキチン化には，標的のリジン残基に対してユビキチン 1 分子が結合するモノユビキチン化と，複数のユビキチン分子が鎖を形成するポリユビキチン化がある。ユビキチン分子自身には，7 箇所のリジン残基と N 末端のメチオニン残基の，合計 8 箇所のユビキチン結合サイトが存在するため，ポリユビキチン化には様々なタイプがある。例えば，48 番目や 11 番目のリジン残基を介してユビキチンが結合した K48 鎖や K11 鎖による修飾はプロテアソーム分解の標識となるのに対して，63 番目のリジン残基を介した K63 鎖は，DNA 修復やエンドサイトーシスなど，多様なシグナルとして働く。様々な文脈で重要な役割を担うユビキチン化であるが，この修飾を触媒するのが，ユビキチンリガーゼと呼ばれる酵素である。

シロイヌナズナゲノムには 1000 を超えるユビキチンリガーゼがコードされており，それらが特異的な標的の制御を介して多様な生理機能に関わることが報告されてきた。当研究室では，シロイヌナズナの膜貫通型ユビキチンリガーゼ ATL31 を栄養応答の重要な制御因子として同定し，解析を進めていた。栄養の中でも，炭素(C)と窒素(N)は代謝の根幹を成す因子であり，その相対量が植物の

生育に影響を与える。例えば，炭素が多く窒素が少ない条件は植物にとってストレスとなり，発芽後成長の抑制や，老化の促進が起きる。ATL31 の過剰発現体は高 C/低 N 栄養ストレスに対して非感受性を示し，機能欠損変異体は高感受性を示す。先行研究により，ATL31 は 14-3-3 タンパク質をユビキチン化して分解に導くことで，高 C/低 N 栄養ストレス条件における植物の生育を可能にしていることが分かっていた。しかし，ATL31 の細胞内における局在パターンや輸送制御については未解明であった。そこで，本研究では，ATL31 の局在制御に着目し，植物の C/N 栄養応答制御機構の解明を目指して解析を開始した。

まず初めに，共焦点顕微鏡を用いた細胞内局在解析により，ATL31 がトランスゴルジ網/初期エンドソーム (TGN/EE) と細胞膜との間を行き来し，液胞へと輸送されて分解されることを明らかにした。さらに，生化学的な解析により，ATL31 の相互作用因子として SYNTAXIN OF PLANTS 61 (SYP61) という，TGN/EE 局在型の SNARE タンパク質（Soluble N-ethylmaleimide sensitive factor attachment protein receptor）を同定した。SNARE タンパク質は，輸送小胞と標的膜の間で SNARE 複合体を形成することで膜融合を実行する，膜交通の制御因子である。*syp61* 機能抑制変異体では，ATL31 が異常な局在パターンを示したことから，ATL31 の正常な局在制御には，SYP61 を必要とすることが分かった。この *syp61* 機能抑制変異体は，高 C/低 N 栄養ストレスに対して高感受性を示し，ATL31 過剰発現によるストレス耐性を抑制したことから，SYP61 による ATL31 の正常な局在制御が，ATL31 を介した高 C/低 N 栄養応答に必要であると考えられる。一方で，リコンビナントタンパク質を用いた *in vitro* アッセイと，植物体における一過的な共発現系から，ATL31 が SYP61 をユビキチン化できることが分かった。さらに，K63 鎖を含む SYP61 のユビキチン化は，低 C/高 N 栄養条件誘導的に一過的に促進されることが明らかとなった。この低 C/高 N 栄養条件誘

導的な SYP61 のユビキチン化は，*ATL31* 過剰発現体において増強されたが，一方で *atl31* とそのホモログ *atl6* の多重機能欠損変異体背景では減少しなかった。このことから，ATL31 は SYP61 をユビキチン化できるが，ATL31 の他にもこの修飾を行うユビキチンリガーゼが存在することが分かった。ユビキチン K63 鎖はエンドサイトーシスのシグナルとなることが知られており，SYP61 は細胞膜にも観察されることから，ユビキチン化が SYP61 の細胞膜からの取り込み促進に寄与する可能性について検証した。その結果，SYP61 の細胞膜局在は，低 C/高 N 条件では減少したものの，ATL31 過剰発現による影響は見られなかった。このことから，少なくとも ATL31 による SYP61 のユビキチン化は，エンドサイトーシスのシグナルにはならないと考えられる。酵母や動物においては, SNARE タンパク質のユビキチン化が，プロテアソーム分解や液胞分解などの他，分解ではない局在制御のシグナルになる例や，SNARE 複合体形成の制御に関わる例などが，近年いくつか報告されてきている。一方，植物では，ユビキチン化タンパク質の網羅解析において, 細胞膜局在型の SNARE タンパク質が検出されたという報告に留まっていた。SYP61 ユビキチン化の下流については，今後の詳細な解析が必要だが，本研究の結果から，植物の栄養応答において，SNARE タンパク質がユビキチン化による機能制御を受けることが示唆された。

以上のように，本研究によって，植物の C/N 栄養応答において SNARE タンパク質が重要な役割を果たすことが明らかとなったことに加え，植物の栄養応答における，SNARE タンパク質のユビキチン修飾を介した制御という新たな可能性が示された。

ACKNOWLEDGEMENTS

Firstly, I would like to express my sincere gratitude to my supervisors Dr. Junji Yamaguchi and Dr. Takeo Sato for their devoted guidance, valuable advice, giving me a lot of chance to meet and discuss with other researchers, and all their support throughout my lab life.

I would like to sincerely thank Dr. Tomohiro Uemura and Dr. Akihiko Nakano for technical support, providing the materials and advice. To Dr. Uemura, I also thank you for allowing me a short stay at your lab to perform experiments. I am also grateful to Dr. Yutaro Shimizu for technical support during this stay.

I would like to extend my sincere gratitude to Dr. Anirban Baral and Dr. Rishikesh P. Bhalerao for providing the SYP61 amiRNA seeds and valuable advice. Your warm encouragement and strong technical support enabled me to get through my PhD.

I would like to deeply thank Dr. Yohann Boutté for giving me the chance to join your lab for half year, teaching me technics, and supporting me. I would like to express my warm thanks also to Dr. Yoko Ito, Dr. Nicolas Esnay, Dr. Valérie Wattelet-Boyer, Dr. Adiilah Mamode Cassim, Dr. Anne-Flore Deroubaix, and Dr. Florence Corellou for your friendship and supporting me both technically and mentally during this stay. My sincere thanks also go to the Bordeaux Imaging Center and Dr. Stephane Claverol for technical support.

I would like to greatly thank Dr. Yoichiro Fukao for ATL31 interactome analysis, Dr. Emi Ito, Dr. Kazuo Ebine, Dr. Ooi Kock Teh, and Nikon Imaging Center at Hokkaido University for helpful advice and technical support for microscopic analysis, Dr. Yasushi Saeki and Dr. Keiji Tanaka for mass spectrometry analysis of ubiquitin chain-type, the Instrumental Analysis Division, Global Facility Center, Creative Research Institution, Hokkaido University for mass spectrometry analysis for identification of SYP61 ubiquitination site, and Dr. Tsuyoshi Nakagawa, Dr. Shoji Mano, Dr. Junpei Takano and Dr. Michael R. Blatt for the Gateway vectors.

For financial support, I am grateful to Japan Society for the Promotion of Science (JSPS) for the JSPS Research Fellowship for Young Scientists, and the Overseas Challenge Program for Young Researchers.

I would like to express my sincere thanks to Dr. Shigetaka Yasuda who taught me experimental technics and lab tips when I joined this lab and also after he left.

I am deeply grateful to Dr. Thais Huarancca Reyes who helped me with starting this study, and gave me important technical advice.

I would like to express my heartfelt thanks to Akari Fujimaki, Yongming Luo, Mayu Arai, Hitomi Sekihara, and Yoshie Morita for technical support, and warm friendship.

I greatly appreciate Dr. Junpei Takagi for giving me useful advice on imaging technics and text editing.

I would like to greatly thank Dr. Kazuma Tanaka and Dr. Tomomichi Fujita for their useful advice.

I would like to express my sincere thanks to Dr. Shoki Aoyama who instructed me in writing and presentation.

I would like to extend my heartfelt appreciation to all current and former members of the lab and my friends for their friendship and support.

My sincere thanks also go to Christopher Lai who instructed me in English writing.

Lastly but not least, I would like to thank my family, Hitomi, Yasuhiro, Tomoaki, and Rintaro for their support and encouragement.

SUMMARY

Ubiquitination is a post-translational modification with reversible attachment of the small protein ubiquitin, which is involved in numerous cellular processes including membrane trafficking of cargo proteins. However, ubiquitination of the trafficking machinery components and their involvement in environmental responses remains elusive. Here, I demonstrated Arabidopsis *trans*-Golgi network/early endosome (TGN/EE) localized soluble *N*-ethylmaleimide sensitive factor attachment protein receptor (SNARE) protein SYP61 as a novel interactor of a transmembrane ubiquitin ligase ATL31, which was previously reported as a key regulator of the stress resistance to disrupted carbon (C)/nitrogen (N)-nutrient conditions. SYP61 is a key component of membrane trafficking in Arabidopsis. The subcellular localization of ATL31 was disrupted in the knockdown mutants of *SYP61*, and the high C/low N-stress insensitivity of the ATL31 overexpressor was repressed in these mutants, suggesting their cooperative function in plant responses to nutrients. I also demonstrated SYP61 is ubiquitinated in plants, and the ubiquitination level was up-regulated in low C/high N-nutrient conditions. Our results provided new insights into the ubiquitin signaling and membrane traffic machinery in plant physiology.

INTRODUCTION

Ubiquitination plays critical roles in regulating various proteins and enables flexible responses toward the changing environment (Hershko and Ciechanover, 1998; Oh et al., 2018). Ubiquitin is an 8.5 kDa protein, which is attached to lysine (K) residues of target proteins by ubiquitin ligases. As ubiquitin can form chain through its own seven K and one N-terminal methionine residues, there are several types of topologically different

ubiquitin chains, which modulate distinct cellular processes (Oh et al., 2018). For example, proteins modified by compact structured K48 and K11-linked ubiquitin chains undergo proteasomal degradation, whereas more flexible K63-linked ubiquitination is involved in several processes, including vacuolar targeting, endocytosis, DNA repair and signal activation (Callis, 2014; Isono and Kalinowska, 2017; Oh et al., 2018; Romero-Barrios and Vert, 2018). Protein ubiquitination is involved in regulating the membrane trafficking of cargo proteins during plant responses to environmental stresses. For example, multiple mono-ubiquitination of the plant metal transporter IRON-REGULATED TRANSPORTER 1 (IRT1) is necessary for its constitutive turnover from the plasma membrane to the TGN/EE, with extension of ubiquitination into K63-linked chains in the presence of excess amounts of non-iron metal ions leading to vacuolar degradation (Barberon et al., 2011; Dubeaux et al., 2018). Ubiquitination of other plasma membrane localized proteins, including brassinosteroid receptor BRASSINOSTEROID INSENSITIVE 1 (BRI1), and auxin efflux carrier PIN FORMED 2 (PIN2), also triggers endocytosis and vacuolar targeting (Leitner et al., 2012; Korbei et al., 2013; Martins et al., 2015; Zhou et al., 2018). Ubiquitination of boron transceptor REQUIRES HIGH BORON 1 (BOR1) was reported to be necessary for its vacuolar degradation under high concentration of boron (Kasai et al., 2011; Yoshinari et al., 2020), and mono-ubiquitination of a membrane associated receptor-like cytoplasmic kinase BOTRYTIS-INDUCED KINASE 1 (BIK1) was recently reported to trigger its endocytosis and plays important role for activation of plant immunity (Ma et al., 2020). Deubiquitination reactions are also important for the cargo protein trafficking via the ESCRT system (Isono and Kalinowska, 2017). Although these previous studies showed trafficking regulation of cargo proteins, less is known about the ubiquitination

of the trafficking machinery itself.

SNARE proteins are key regulators of membrane trafficking, which are conserved among eukaryotes (Jahn and Scheller, 2006; Lipka et al., 2007; Wickner and Schekman, 2008). They mediate vesicle fusion by forming SNARE complexes, consisting of four different types of SNARE motifs, Qa-, Qb-, Qc-, and R-SNARE. The Arabidopsis genome encodes more than 60 SNARE proteins (Sanderfoot et al., 2000; Uemura et al., 2004; Lipka et al., 2007; Sanderfoot, 2007). Each SNARE protein localizes to specific membranes, and has specific SNARE partners in the cells (Pratelli et al., 2004; Uemura et al., 2004; Jahn and Scheller, 2006; Fujiwara et al., 2014). Some SNARE proteins are reported to have several different SNARE partners and mediate different trafficking pathways. For example, a TGN/EE localized Qc-SNARE protein, SYNTAXIN OF PLANTS 61 (SYP61) is reported to mediate vacuolar trafficking with SYP41 (Qa-SNARE), VPS TEN INTERACTING 12 (VTI12, Qb-SNARE), and a Sec1/Munc18 (SM) family protein, VACUOLAR PROTEIN SORTING 45 (VPS45) (Zouhar et al., 2009; Kim and Bassham, 2011), and retrograde and anterograde trafficking of aquaporin PLANT PLASMA MEMBRANE INTRINSIC PROTEINS 2;7 (PIP2;7), possibly with SYP121 (Qa-SNARE) (Hachez et al., 2014). SYP61 is also reported to mediate exocytotic trafficking of cell wall components (Drakakaki et al., 2012; Gendre et al., 2013). SNARE proteins play important roles in plant physiological responses. For *SYP61*, the knockdown mutant was previously reported to be hypersensitive to the salt and osmotic stresses (Zhu et al., 2002).

Sugar (carbon, C) and nitrogen (N) are essential components of organisms, and their relative availability, C/N-nutrient balance, affects many aspects of plant physiology. For example, excess sugar with limited nitrogen in early post-germination stage inhibit the

seedling growth with accumulation of anthocyanin, and high CO_2/low N conditions in mature stages promote the progression of senescence in Arabidopsis plants (Coruzzi and Zhou, 2001; Martin et al., 2002; Aoyama et al., 2014a, 2014b). Those high C/low N-nutrient stress phenotypes are rescued by either reducing the amount of carbon sources or enhancing that of nitrogen. A previous report from my colleagues suggested the T6P (Trehalose 6-Phosphate)-SnRK1 (SNF1- related protein kinase 1 complex) module mediates the C/N-nutrient signaling (Li et al., 2020). T6P is an intermediate metabolite of trehalose biosynthesis, and inhibits the activity of SnRK1 by directly binding to the SnRK1α subunit (Zhai et al., 2018). Previous researches have also reported a membrane localized ubiquitin ligase ARABIDOPSIS TOXICOS EN LEVADURA 31 (ATL31) as a downstream target of the SnRK1-regulated kinases, *CBL-INTERACTING PROTEIN KINASEs 7*, *12*, and *14* (*CIPK7/12/14*) (Yasuda et al., 2017; Li et al., 2020). ATL31 enhances plant high C/low N-nutrient stress tolerance through targeting 14-3-3 proteins for proteasomal degradation by binding them through the CIPK7/12/14-mediated phosphorylation (Sato et al., 2009, 2011; Yasuda et al., 2014, 2017).

In this study, I identified SYP61 as a novel interactor of ATL31. I demonstrated SYP61 is necessary for the proper localization of ATL31 and the ATL31-mediated C/N-nutrient stress responses. I also found SYP61 is ubiquitinated in plants, and the ubiquitination level was regulated in response to C/N-nutrient availabilities, further opening the possibilities of SNARE regulations in nutrient responses.

MATERIALS AND METHODS

Plant material and growth conditions

The *Arabidopsis thaliana* ecotypes Columbia-0 (Col-0) and C24 were used in this study. The T-DNA insertion mutant *osm1* (Zhu et al., 2002) was kindly provided by Dr. Jianhua Zhu (University of Maryland). The T-DNA insertion mutants *atl31-1* and *atl6-1* are characterized previously (Sato et al., 2009). Transgenic Arabidopsis plants, *2xp35S:ATL31-GFP*, *pSYP61:GFP-SYP61*, *p35S:ST-mRFP*, *pSYP61:mRFP-SYP61*, *pSYP43:mRFP-SYP43*, *pVHAa1:VHAa1-mRFP*, *pARA7:mRFP-ARA7* and *pVAMP727:tagRFP-VAMP727* have been described (Fecht-Bartenbach et al., 2007; Sato et al., 2009; Uemura et al., 2012; Inada et al., 2016; Shimizu et al., 2021). *pVHAa1:VHAa1-mRFP* was kindly provided by Dr. Karin Schumacher (Heidelberg University, Germany). The SYP61 amiRNA constitutive-expressing or inducible lines are kind gift from Drs. Anirban Baral and Rishikesh P. Bhalerao. Co-expression lines were generated by crossing, and F1 or homozygous lines of F3 generation were used for microscopic observation and carbon/nitrogen-nutrient response analysis. For seed amplification, Arabidopsis seeds were surface-sterilized and sowed on 1x Murashige and Skoog (MS) medium supplemented with 1% sucrose, vitamins and 0.4% gellan gum (pH5.7). After kept in dark at 4°C for 2-4 days to synchronize germination, the plants were grown under 16 hours light/8 hours dark at 22°C on the plates for several weeks, and transferred to flowerpot with soil containing compost and vermiculate in the ratio of 1:6. Tap water was used for watering. *Nicotiana benthamiana* plants were used for transient protein expression. The surface-sterilized seeds were sowed on 1xMurashige and Skoog (MS) medium supplemented with 1% sucrose, vitamins and 0.4% gellan gum (pH5.7), and grown under 16 hours light/8 hours dark at 22°C on the

plates for two weeks, then transferred to flowerpot with soil containing compost and vermiculate in the ratio of 1:6. Tap water was used for watering, and supplied with 1/1000 diluted Hyponex (HYPONeX JAPAN CORP, Japan) once a week.

For microscopy imaging of Arabidopsis root cells, seeds were vertically grown on modified Murashige and Skoog (MS) medium containing 100 mM glucose, 30 mM nitrogen (10 mM NH_4NO_3 and 10 mM KNO_3), vitamins and 0.8% agar (pH5.7). The preparation protocol of the modified MS medium has been described (Sato et al., 2009; Huarancca Reyes et al., 2018). For vacuolar accumulation analysis, *2xp35S:ATL31-GFP* seedlings were wrapped in a double layer of aluminum foil 18 hours before the observation, and the 6 day-old plants were observed. For microscopy with *syp61* inducible amiRNA lines, plants were grown for 7 days on the modified MS medium containing 50 mM glucose, 30 mM nitrogen (10 mM NH_4NO_3 and 10 mM KNO_3), vitamins and 0.8% agar (pH5.7) supplied with 10 μM of β-estradiol or equal amount of ethanol.

For the detection of the ubiquitination of SYP61 in Arabidopsis, seeds were grown in liquid 1xMS medium supplemented with 1% sucrose and vitamins (pH5.7) for 10 days under constant light with shaking at 70 rpm.

To test the effect of C/N-nutrient conditions on SYP61 ubiquitination, seeds were grown in modified MS liquid medium containing 100 mM glucose, 30 mM nitrogen (10 mM NH_4NO_3 and 10 mM KNO_3), vitamins and 2 mM MES (pH5.7) for 10 or 11 days under constant light with shaking at 70 rpm, and treated with various MS medium containing different concentration of glucose, nitrogen and mannitol for the indicated time.

Transient expression in *Nicotiana benthamiana*

For the plasmid construction, coding sequences of each gene were amplified by PCR and cloned into vector pENTR/D-TOPO (Life Technologies). These fragments were subsequently transferred to destination vectors using the Gateway system according to the manufacturer's protocol (Invitrogen). For immunoprecipitation assays, coding sequences of *ATL31* and *ATL31*^{C143S} were subcloned into the pGWB11 destination vector, and *SYP61* (At1g28490) was subcloned into pGWB6 and pGWB12 destination vectors (Nakagawa et al., 2007). For the *in vivo* ubiquitination analysis, coding sequences of *ATL31* and *ATL31*^{C143S} were transferred into the pAMPAT-GW-3xFLAG destination vector (Yamada et al., 2016), and using them as templates, the sequences from *ATL31* or *ATL31*^{C143S} to *3xFLAG* were subcloned into the pGWB502-Ω destination vector (Nakagawa et al., 2007). The primers are listed in Supplemental Table 1. All constructs were introduced into *Agrobacterium tumefaciens* strain GV3101 (pMP90) by electroporation. The *A. tumefaciens* containing the constructs were grown in 2xYT liquid medium at 28°C overnight with shaking, and the cells were resuspended with infiltration buffer (10 mM MES, 10 mM $MgCl_2$, and 450 μM acetosyringone, pH 5.6). The mixtures of the suspension were infiltrated into the leaves of 5-6-week-old *N. benthamiana* by syringe without needle. The *A. tumefaciens* carrying p19 suppressor was co-infiltrated with the all samples (Takeda et al., 2002). After 3 days, the leaves were harvested with liquid nitrogen.

Western blotting analysis of ATL31-GFP after Concanamycin A treatment

The transgenic plants *2xp35S:ATL31-GFP* were grown in the modified MS liquid medium containing 100 mM glucose, 30 mM nitrogen (10 mM NH_4NO_3 and 10 mM

KNO_3), vitamins and 2 mM MES (pH5.7) for 10 days under constant light with shaking at 70 rpm, and treated with the medium supplied with 1 μM Concanamycin A (SIGMA-ALDRICH, C9705) or the same amount of DMSO (1:200 dilution) for 3 hours. The plants were frozen by liquid nitrogen and powdered with stainless steel beads. About 6 μL/mg-FW of 1xSDS-sample buffer was directly added to the samples. The 1xSDS was prepared by diluting 2x solution (125 mM Tris-HCl (pH6.8), 4% SDS, 20% glycerol, 10% 2-mercaptoethanol, 0.02% bromophenol blue) by protein extraction buffer (50 mM Tris-HCl (pH7.5), 0.5% Triton X-100, 150 mM NaCl, 10% glycerol, 1 mM EDTA, pH 7.5). The extracts were incubated at 55°C for 40 minutes, and the debris were removed by centrifugation at 20,000xg 5 minutes for twice. Proteins were separated by SDS-PAGE and detected by immunoblotting with anti-GFP (MBL, 598) and anti-alpha-Tubulin (DM1A) (Calbiochem, CP06-100UGCN). CBB staining was performed using AE-1340 EzStain AQua (ATTO, 2332370) according to the manufacturer's protocol. The band intensity of the full-length ATL31-GFP and the free GFP was quantified by ImageJ software (National Institutes of Health, Maryland, Washington, DC), and the ratio was calculated.

Immunoprecipitation

The plant materials were frozen with liquid nitrogen, and powdered using mortars and pestles, and the expressed proteins were extracted using protein extraction buffer (50 mM Tris-HCl (pH7.5), 0.5% Triton X-100, 150 mM NaCl, 10% glycerol, 1 mM EDTA) supplemented with 10 μM MG132 and Complete Protease Inhibitor Mixture (Roche Applied Science). To detect ubiquitination, the deubiquitination inhibitors 20 mM N-ethylmaleimide and 2 mM 1,10-phenanthroline were added. To test the *in planta*

ubiquitination of SYP61 by ATL31, and the effect of C/N-nutrient conditions, 500 nM of MLN-7243 (other name, TAK-243) (Active Biochem, A-1384) was also added as an E1 inhibitor to avoid additional ubiquitination during the extraction steps. The mixtures were centrifuged at 20,000x*g* for 5 minutes at 4°C and the supernatants were collected. This step was repeated twice, and then the proteins were immunoprecipitated with anti-FLAG M2 affinity gel (Sigma-Aldrich, M8823), anti-GFP mAb-magnetic agarose (MBL, D153-10), anti-GFP mAb-Magnetic Beads (MBL, D153-11) or anti-RFP mAb-Magnetic Beads (MBL, M165-11). D153-11 was used for checking ubiquitination of GFP-SYP61 in response to C/N-nutrient conditions, and D153-10 was used for other experiments to immunoprecipitate GFP-tagged proteins. The extracts and the beads were mixed and rotated at 4°C for 1 hour, and washed for more than three times with the extraction buffer without inhibitors. To detect FLAG-SYP61 ubiquitination, proteins were eluted with 150 $\mu g.ml^{-1}$ 3× FLAG peptide (Sigma-Aldrich, F4799) in extraction buffer, followed by precipitation in cold acetone, resuspension in SDS sample buffer (62.5 mM Tris-HCl (pH6.8), 2% SDS, 10% glycerol, 5% 2-mercaptoethanol, 0.01% bromophenol blue) and incubation at 90°C for 5 minutes. In other experiments, proteins were eluted with the SDS sample buffer at 90°C for 5 minutes or 55°C for 30 minutes.

Proteins were separated by SDS-PAGE and detected by immunoblotting with anti-FLAG (SIGMA-ALDRICH, F1804-200UG), anti-SYP61, anti-GFP (MBL, 598), anti-mCherry (Clontech, 632543), anti-ubiquitin (FK2) (Wako, 302-06751), anti-K48 ubiquitination (Apu2) (Millipore, 05-1307) and anti-K63 ubiquitination (Apu3) (Millipore, 05-1308) antibodies. Anti-SYP61 antibody is a kind gift from Drs. Tomohiro Uemura (Ochanomizu University) and Akihiko Nakano (RIKEN). The detection specificity of the antibody was confirmed (Fig. 1). The band intensity was quantified by

ImageJ software (National Institutes of Health, Maryland, Washington, DC).

Split ubiquitin yeast two-hybrid assay

All assays used the yeast strain L40ccua (*MATa his3Δ200 trp1-901 leu2-3,112 LYS2::*(lexAop)$_4$-*HIS3 ura3::*(lexAop)$_8$-*lacZ ADE2::*(lexAop)$_8$-*URA3 gal80* can^R cyh2^R). The full-length coding sequences of *ATL31* and *ATL31*^{C143S} were subcloned into the destination vector pMetYC_GW, containing the C-terminal half of ubiquitin, and the full-length coding sequence of *SYP61* was subcloned into the destination vector pNX32_GW, containing the N-terminal half of ubiquitin (Obrdlik et al., 2004). The empty vector pNX32_GW was used as a negative control. Constructs were transfected into yeast using Frozen-EZ Yeast Transformation II Kits (Zymo Research) according to the manufacturer's protocol, with growth assessed as described in the Yeast Protocols Handbook (Clontech).

Recombinant protein expression and purification for *in vitro* ubiquitination assay

GST-tagged truncated SYP61, which included amino acid residues 1 to 218, was expressed in *E. coli* strain BL21(DE3) pLysS (Novagen), and purified with Glutathione-Sepharose 4B (GE Healthcare, 17-0756-01) following the manufacturer's protocol.

***In vitro* ubiquitination assay**

In vitro ubiquitination assays were performed as described (Sato et al., 2009) with some modifications. For Quantitative ubiquitin chain type analysis with AQUA peptide, 500 ng of MBP-ATL31 was incubated for 0-3 hours at 30°C in 30 μL of reaction mixture

containing 50 ng E1 (Wako, 219-01111), 50 ng UbcH5a for E2 (Wako, 215-01191), 4 μg ubiquitin (Sigma-Aldrich, U6253), 25 μM MG132, 40 mM Tris-HCl (pH 7.5), 5 mM $MgCl_2$, 2 mM ATP and 2 mM DTT. For GST-SYP61 ubiquitination analyses, 500 ng of GST-SYP61 or GST were incubated with 500 ng of MBP-ATL31 for 0-3 hours at 30°C in 30 μL of reaction mixture containing 50 ng E1 (Wako, 219-01111), 51 ng UbcH5a for E2 (Wako, 215-01191), 4 μg ubiquitin (Sigma-Aldrich, U6253), 25 μM MG132, 40 mM Tris-HCl (pH 7.5), 5 mM $MgCl_2$, 2 mM ATP and 2 mM DTT. For the ubiquitination assays with mutated ubiquitins, 500 ng of GST-SYP61 or GST were incubated with 500 ng of MBP-ATL31 for 0-1 hours at 30°C in 30 μL of reaction mixture containing 200 nM E1 (R&D Systems, E-305-025), 250 ng UbcH5a for E2 (Wako, 215-01191), 6 μg ubiquitin proteins (native ubiquitin: Ubiquitin human, U-100H, Boston Biochem; K63R ubiquitin: rhUbiquitin K63R, UM-K63R, Boston Biochem; K63 only ubiquitin: rhUbiquitin K63 only, UM-K630, Boston Biochem), 25 μM MG132, 40 mM Tris-HCl (pH 7.5), 5 mM $MgCl_2$, 2 mM ATP and 2 mM DTT. Reactions were stopped by adding the same amount of 2x SDS sample buffer (125 mM Tris-HCl (pH6.8), 4% SDS, 20% glycerol, 10% 2-mercaptoethanol, 0.02% bromophenol blue). Proteins were separated by SDS-PAGE and detected by immunoblotting using anti-MBP (New England BioLabs, E8032S), anti-GST (MBL, M071-3), anti-ubiquitin (FK2) (Wako, 302-06751), anti-K48 ubiquitination (Apu2) (Millipore, 05-1307) and anti-K63 ubiquitination (Apu3) (Millipore, 05-1308) antibodies.

Mass spectrometry analysis of ubiquitination sites

Ubiquitinated GST-SYP61 proteins were separated by SDS-PAGE and stained with SYPRO Ruby (Lonza, Switzerland) as described in the manufacturer's protocol. Gel

pieces containing ubiquitinated GST-SYP61 were excised, dehydrated with 100% acetonitrile and incubated in 10 mM dithiothreitol and 50 mM ammonium bicarbonate for 45 minutes at 56°C with shaking. The gel pieces were subsequently incubated in 55 mM chloroacetamide/50 mM ammonium bicarbonate for 30 minutes at room temperature, washed with 25 mM ammonium bicarbonate and dehydrated with 100% acetonitrile. The dried gels were incubated for 16 hours at 37°C in 50 mM ammonium bicarbonate containing sequence grade modified trypsin (Trypsin Gold; Promega, USA). The digested peptides were eluted from the gels with 50% acetonitrile (v/v) /5% formic acid (v/v) and dried using an evaporator. The peptides were dissolved in 2% acetonitrile (v/v) /0.1% formic acid (v/v) and filtered with Ultrafree-MC Centrifugal Filters (PVDF 0.45 μm; Millipore, USA). Peptides were identified using an EASY-nLC 1000 liquid chromatograph coupled to an Orbitrap Mass Spectrometer (Thermo Scientific, USA), followed by assessment using a SEQUEST algorithm embedded in Proteome Discoverer 1.4 software (Thermo Scientific, USA) against TAIR10 (http://www.arabidopsis.org/index.jsp), as described (Lu et al., 2016).

Gene expression analysis

Total RNA was isolated from the 7-days-grown Arabidopsis seedlings using TRIzol reagent (Invitrogen), and was treated with RQ1 RNase-free DNase (Promega) according to the manufacturer's protocols. Then, the cDNA was synthesized using oligo(dT) primer (Promega) with *18S rRNA* specific primer and ReverTraAce reverse transcriptase (Toyobo). qRT–PCR analysis was performed using SYBR premix Ex Taq (TaKaRa) and Mx3000P (Agilent Technologies) according to the manufacture's protocol. The used primers are listed in Supplemental Table 2.

Carbon/nitrogen-nutrient response analysis

Seeds of each genotype were surface-sterilized and sown on modified MS-based solid medium containing 0.4% gellan gum, vitamins, glucose, mannitol and nitrogen (KNO_3 and NH_4NO_3 were used in 1:1 molar ratio) at the concentration indicated in figures. The medium was prepared as described (Sato et al., 2009; Huarancca Reyes et al., 2018). 10 μM of β-estradiol or equal amount of ethanol was added in the medium for the experiment with *syp61* inducible amiRNA lines. After kept in dark at 4°C for 2 days to synchronize germination, the plants were grown under 16 h light/8 h dark at 22°C. The percentage of the seeds with green cotyledons in the germinated seeds were calculated.

Chemical treatment for microscopy

5 or 6 day-old seedlings were incubated in the modified liquid MS medium 100 mM glucose/30 mM nitrogen containing 50 μM Brefeldin A (BFA), or 33 μM Wortmannin (WM). Fluorescence was monitored by confocal microscopy 30 minutes and 1 hour later respectively. Seedlings treated with BFA were pre-incubated in 5 μM FM4-64 dye for 15 minutes and then transferred to BFA containing medium.

For Concanamycin A treatment, 7 day-old seedlings were incubated in the modified liquid MS medium 100 mM glucose/30 mM nitrogen containing 1 μM Concanamycin A (SIGMA-ALDRICH, C9705) or the same amount of DMSO (1:200 dilution), and observed using confocal microscopy after 3 hours.

FM4-64 internalization assay

7 day-old seedlings were pulse-stained with 2 μM FM4-64 dye in the modified liquid

MS medium 100 mM glucose/30 mM nitrogen for 2 minutes, washed twice with the dye-free medium, and subjected to microscopy observation.

C/N-nutrient treatment for microscopy

For the colocalization analysis of ATL31-GFP and the organelle markers, 6 day-old seedlings were treated with the modified liquid MS medium containing indicated amount of glucose and nitrogen, and observed 90-110 minutes after the treatment. For the plasma membrane localization analysis of mRFP-SYP61, 5 day-old plants were subjected to overnight treatment, and the 6 day-old seedlings were observed.

Confocal laser-scanning microscopy

Confocal laser-scanning microscopy was performed using Zeiss LSM510 equipped with C-Apochromat 40x/1.20 W Korr UV-VIS-IR lens, LSM980 with Plan-Apochromat 63×/NA 1.4 Oil objective lens, and Nikon Ti-E inverted microscope equipped with Plan Apo λ 60x Oil lens and a Nikon A1Rsi spectral imaging confocal scanning system. For the observation with the Zeiss LSM510 microscope, GFP fluorescence was excited by a 488 nm laser and detected using a 505–550 nm band-pass emission filter, whereas RFP fluorescence was excited by a 561 nm laser and detected using a 575–615 nm band-pass emission filter. FM4-64 fluorescence was excited by a 561 nm DPSS laser and detected using a 575 nm long-pass emission filter. For the observation with the Zeiss LSM980 microscope, fluorescence was excited by a 488 nm laser for GFP and 543 nm for RFP, and the fluorescence emissions were detected at 490-543 nm for GFP and 596-694 nm for RFP. For the observation with Nikon microscope system, GFP fluorescence was excited by a 488 nm laser and detected using a 500–550 nm band-pass emission filter,

and RFP and FM4-64 fluorescence were excited by a 561 nm laser and detected using a 570-620 nm band-pass emission filter. Images were processed using ImageJ software (National Institutes of Health, Maryland, Washington, DC).

Colocalization analysis

Object-based distance analysis was performed by ImageJ plugin DiAna (Gilles et al., 2017). To remove the noise, a median filter of 2 pxl-radius was applied before analysis. For the analysis of plants without treatments, the dot-like structures were segmented by DiAna-segmentation with the following parameters: spot segmentation; RadXY, 3; RadZ, 1; Noise, 50; Radius Max (pxl), 7; sd value, 1.4; volume min (pxl), 4; volume max (pxl), 200; exclude objects on XY edges, yes; seed threshold, 3000 for ATL31-GFP, 2000 for ST-mRFP, 4000 for VHAa1-mRFP, 3000 for mRFP-SYP43, 2800 for mRFP-SYP61, 3000 for tagRFP-VAMP727, and 3500 for mRFP-ARA7. For the analysis of plants with C/N-nutrient liquid medium treatments, the following parameters were used: spot segmentation; RadXY, 3; RadZ, 1; Noise, 50; Radius Max (pxl), 7; sd value, 1.4; volume min (pxl), 4; volume max (pxl), 200; exclude objects on XY edges, yes; seed threshold, 5500 for ATL31-GFP, 4500 for VHAa1-mRFP and tagRFP-VAMP727. The segmented objects with signal at the plasma membrane and the outside of the cell of interest were removed manually. After the segmentation, the distance of the centroids of the closest neighbor was measured by DiAna-analysis. The objects with the center-center distance shorter than the theoretical resolution were considered as colocalizing. The optical resolution was considered as 0.2 μm here (according to the Rayleigh criterion, the theoretical lateral resolution was calculated by the following formula: 0.51λ/NA (λ, excitation wavelength; NA, numerical aperture of

the objective lens) = 0.51*543/1.40 = 197.8 nm < 0.2 μm). n = 15 cell slices from 5 roots were analyzed.

Dot/cytosol intensity ratio analysis of ATL31-GFP

ImageJ was used for the analysis. A median filter of 2 pxl-radius was applied to remove the noise. The dot-like structures of ATL31-GFP were segmented by DiAna with the following parameters: spot segmentation; RadXY, 3; RadZ, 1; Noise, 50; Radius Max (pxl), 7; sd value, 1.4; volume min (pxl), 4; volume max (pxl), 200; exclude objects on XY edges, yes; seed threshold, 16000. The intracellular region excluding the dot-like structures was considered as cytosol in this analysis. The original images were used for the measurement. The ratio of the mean intensity of the cytosol and the total area of the dot-like structures was calculated. n = 15 cell slices from 5 roots were analyzed.

PM/Dot intensity ratio analysis of mRFP-SYP61

ImageJ was used for the analysis. A median filter of 2 pxl-radius was applied to remove the noise The dot-like structures of mRFP-SYP61 were segmented by DiAna with the following parameters: iterative thresholding, Volume min (pxl), 10; Volume Max (pxl), 200; min Threshold, 200; STEP value, 50. The plasma membrane was selected manually by selection brush tool. The original images were used for the measurement. The ratio of the mean intensity of the plasma membrane and the dot-like structures was calculated. The mean intensity of the dot-like structures was calculated by dividing the total intensity of the dot-like structures by their total area. n = 20 cell slices from 5 roots were analyzed.

Statistics

All values shown as bar graphs are mean ± s.d. or s.e.m. as stated. *P* values were calculated by two-tailed Welch's *t*-test for two-group comparisons, by two-tailed Dunnett's test for multiple-group comparisons with single control, and one-way ANOVA (analysis of variance) followed by Tukey's honestly significant difference (HSD) test for other multiple-group comparisons. Statistical significance was set based on *P*-values. n.s., $P > 0.05$; $*P < 0.05$; $**P < 0.01$.

Accession Numbers

Sequence data from this article can be found in the Arabidopsis Genome Initiative or GenBank/EMBL databases under the following accession numbers: *ATL31*, At5g27420; *SYP61*, AT1g28490; *SYP43*, AT3G05710; *VHAa1*, At2g28520; *ARA7*, AT4G19640; *VAMP727*, AT3G54300.

RESULTS

ATL31 localizes to the plasma membrane and endosomal compartments

Previous researches showed that the N-terminal transmembrane domain of ATL31 is required for ATL31's function in C/N-nutrient stress responses (Sato et al., 2009). To characterize the subcellular localization of ATL31, I performed confocal microscopy observations of Arabidopsis plants expressing green fluorescent protein-tagged ATL31 (ATL31-GFP). In the root tip epidermal cells, ATL31-GFP signals were detected at the intracellular punctate structures and the plasma-membrane (Fig. 2A). The GFP signals colocalized with the internalized FM4-64 dye in less than 20 minutes after staining, suggesting ATL31 localizes to the TGN/EE (Fig. 2A). The identity of these dot-like

structures was further determined by colocalization analysis with monomeric red fluorescent protein (mRFP)- or tagRFP-tagged endomembrane organelle markers in transgenic Arabidopsis plants. As a result, ATL31-GFP colocalized with the TGN/EE markers mRFP-SYP43, mRFP-SYP61 and VHAa1-mRFP (Fig. 2B, C). I also observed the colocalization with the *trans*-Golgi marker ST-mRFP (cytoplasmic and transmembrane domains of a rat sialyl transferase) and the LE markers mRFP-ARA7 and tagRFP-VAMP727 (Fig. 2B, C). Since ST often colocalizes with part of the TGN/EE called Golgi-associated-TGN (GA-TGN) (Uemura et al., 2014; Shimizu et al., 2021), the colocalization of ATL31-GFP with ST-mRFP may indicate its localization at the GA-TGN. To confirm the localization of ATL31 at the TGN/EE and the LE, I also tested the sensitivity of ATL31-GFP on commonly used membrane traffic inhibitors brefeldin A (BFA) and wortmannin (WM). BFA inhibits the BFA-sensitive ADP-ribosylation factors guanine nucleotide exchange factors (Arf-GEFs) and generates BFA bodies, large aggregations of endosomal compartments (Geldner et al., 2003; Grebe et al., 2003; Dettmer et al., 2006; Robinson et al., 2008). The 30 minutes treatment with 50 μM BFA induced the aggregation of ATL31-GFP with fluorescence overlapping FM4-64 containing BFA bodies (Fig. 2D). WM is an inhibitor of phosphoinositide 3-kinase (PI3K) and PI4K, which causes swelling and vacuolization of late endosomal compartments (Jaillais et al., 2008; Wang et al., 2009). After 1 hour of 33 μM WM treatment, ATL31-GFP was observed as small ring-like structures (Fig. 2E). Those pharmacological analyses further supported the finding that ATL31 localizes to the TGN/EE and the LE. Membrane localized proteins often undergo vacuolar degradation, and this can be visualized by the signal of the tagged GFP in the vacuole after dark treatment (Tamura et al., 2003). After 18 hours dark treatment, GFP

fluorescence was observed in vacuoles in addition to the intracellular punctuate structures (Fig. 2F), whereas mRFP-SYP61 was not observed in the vacuole (Fig. 3). The vacuolar targeting of ATL31 was also confirmed by treatment with a vacuolar ATPase inhibitor Concanamycin A (ConcA) (Dröse et al., 1993; Matsuoka et al., 1997; Dettmer et al., 2006) (Fig. 4). After 3 hours treatment of ConcA, ATL31-GFP was observed in abnormal patches and the protein amount ratio of full-length ATL31-GFP to the free GFP was enhanced (Fig. 4). These results suggested ATL31-GFP is subjected to vacuolar degradation in Arabidopsis cells.

Because ATL31 is a C/N-nutrient response regulator, I also checked the subcellular localization of ATL31 under different C/N-nutrient conditions. Transgenic Arabidopsis seedlings expressing ATL31-GFP with the TGN/EE marker VHAa1-mRFP or the LE marker tagRFP-VAMP727 were subjected to liquid medium containing 0 mM glucose (Glc)/60 mM N, 100 mM Glc/30 mM N, or 200 mM Glc/0.3 mM N for 90 to 110 minutes (Fig. 5). The colocalization of ATL31 with VHAa1-mRFP did not show C/N-nutrient condition dependency, possibly because TGN/EE is a trafficking hub that harbors both exocytic and endocytic pathways (Uemura et al., 2014, 2019; Shimizu et al., 2021) . On the other hand, the less dot-like structures of ATL31-GFP colocalized with tagRFP-VAMP727 under higher C/lower N conditions. It has been previously reported that ATL31 is stabilized under higher C/lower N conditions (Yasuda et al., 2017). The less colocalization of ATL31-GFP with the LE marker may indicate the decreased vacuolar targeting of ATL31 under these conditions.

Altogether, ATL31 localizes to the multiple organelles including the plasma membrane, TGN/EE, and LE, and degraded in the vacuole. The observation that the subcellular localization of ATL31 is affected by the C/N-nutrient conditions suggested the relevance

of the regulation of ATL31 trafficking to its function.

ATL31 physically interacts with TGN/EE SNARE SYP61

SYP61 is a Qc-SNARE with N-terminal three helical domains and a C-terminal transmembrane region, that mediates membrane traffic at the TGN/EE in Arabidopsis (Uemura et al., 2004; Sanderfoot et al., 2001). In a proteomic analysis of SYP61 compartment, a protein named ATL6, the closest homologue of ATL31 was identified (Drakakaki et al., 2012). SYP61 is known to mediate the secretion of cell wall components (Drakakaki et al., 2012; Wilkop et al., 2019), and the previous report from my colleagues suggested that ATL31 is also involved in the accumulation of cell wall components (Maekawa et al., 2014). This functional relevance motivated me to evaluate the interaction between ATL31 and SYP61. GFP-tagged SYP61 were transiently co-expressed in *N. benthamiana* leaves with FLAG-tagged ATL31 or the catalytically inactive form of ATL31 with a point-mutation at the conserved cysteine-143 residue in the RING domain to serine ($ATL31^{C143S}$) and subjected to co-immunoprecipitation assay. SYP61 was co-immunoprecipitated with both intact ATL31 and $ATL31^{C143S}$ (Fig. 6A). Physical interactions were confirmed by split ubiquitin yeast two-hybrid analysis done by my previous colleague Dr. Thais Huarancca Reyes (Fig. 6B). In addition, she also detected endogenous SYP61 in the immunoprecipitate of ATL31-GFP from transgenic Arabidopsis plants (Fig. 6C). These results demonstrated that ATL31 physically interacts with SYP61 in plants.

Induced knockdown of *SYP61* affected subcellular localization of ATL31

As SYP61 is a membrane traffic regulator, I observed the subcellular localization of

ATL31 in *syp61* mutants. To examine this, I crossed *ATL31-GFP* expressing plants with two independent lines of the β-estradiol-inducible knockdown mutant of *SYP61*, which express an artificial *SYP61* microRNA (*syp61 Ind amiRNA*). The *syp61 Ind amiRNA* lines are kind gift from Drs. Anirban Baral and Rishikesh P. Bhalerao (Swedish University of Agricultural Sciences). I confirmed the knockdown of *SYP61* was successfully induced under 10 μM β-estradiol existence, while *ATL31* was constitutively overexpressed (Fig. 7A). The seedlings grown on the medium containing 10 μM β-estradiol or ethanol (mock) were observed using confocal laser microscopy (Fig. 7B,C). In the *syp61* knockdown background, fluorescence of ATL31-GFP was more dispersed in the cytosol (Fig. 7B). Quantification showed the mean intensity ratio of cytosol to the dot like structures was significantly enhanced in the mutant (Fig. 7C). This abnormal pattern change upon β-estradiol treatment was not observed in the wild-type background, suggesting this phenotype is caused by the decreased expression of *SYP61*, and not the side-effect of the β-estradiol treatment. These results indicated SYP61 is necessary for the proper localization of ATL31.

SYP61 is required for plant response to disrupted C/N-nutrient balance

I then examined whether SYP61 is involved in the ATL31-mediated high C/low N-nutrient stress responses. Firstly, the high C/low N stress tolerance of *syp61* mutants was tested. The knockdown mutants are kind gift from Drs. Anirban Baral and Rishikesh P. Bhalerao (Swedish University of Agricultural Sciences). The two independent lines of the knockdown mutant plants constitutively expressing the artificial *SYP61* microRNA (*syp61 amiRNA*) (Fig. 8A) showed significant hypersensitive phenotypes to 150 mM Glc/0.3 mM N conditions with no green

cotyledons, whereas 65% of wild-type seedlings showed expanded green cotyledons (Fig. 8B, C). The assay was also performed using *osm1*, a previously reported *syp61* mutant (Zhu et al., 2002). In the *osm1* mutant, the expression pattern of *SYP61* is altered due to the T-DNA insertion in the upstream of the translation start site of *SYP61* (Zhu et al., 2002). Because this mutant is established on a C24 accession background, which was more resistant to high C/low N-nutrient stress, I examined the *osm1* phenotype in medium containing more glucose than the medium used for Col-0 background mutants. In line with the result of *syp61 amiRNA* mutants, the percentage of green cotyledons was significantly lower for *osm1* (10%) than for C24 wild-type (27%) under 300 mM Glc/0.3 mM N stress conditions (Fig. 9). As all wild-type and the *syp61* mutant seedlings showed green cotyledons in mannitol medium, it was confirmed that the effects of C/N-nutrient stress are distinct from that of osmotic stress (Fig. 8,9). Next, to examine the relevance of SYP61 to ATL31 function, I tested the C/N-nutrient stress responses of Arabidopsis plants overexpressing *ATL31* in *syp61* mutant background, which are the same plant lines used for the localization analysis. The crossed plants of *ATL31* overexpressor and the *syp61 Ind amiRNA* were grown on the high C/low N medium containing 300 mM Glc/0.3 mM N with 10 μM β-estradiol or ethanol (mock) (Fig. 10). On the mock medium, the *ATL31* overexpressor and the crossed plants exhibited insensitive phenotype. In contrast, the post-germination growth of the crossed plants was inhibited on the β-estradiol containing stress medium, and the phenotype of the *syp61* knockdown was not rescued by the overexpression of *ATL31*. These results demonstrated that SYP61 plays an essential role in plant adaptation to C/N-nutrient conditions, and is crucial to the ATL31-mediated C/N-nutrient stress insensitivity.

SYP61 protein is ubiquitinated in plant cells

Because ATL31 is a ubiquitin ligase, I also asked the possibility of ubiquitin modification on SYP61. First, I extracted proteins from transgenic Arabidopsis plants expressing GFP-fused SYP61 under the control of native promoter (*pSYP61:GFP-SYP61*). GFP-SYP61 was purified by immunoprecipitation in the absence or presence of inhibitors of deubiquitination enzymes (DUBi). Immunoblotting with anti-GFP antibody detected a signal corresponding to intact GFP-SYP61, whereas immunoblotting with anti-ubiquitin antibody yielded the sharp bands of higher molecular weight, which were enhanced by DUBi treatment (Fig. 11A). Because the predicted molecular size of GFP-SYP61 in this construct is about 55 kDa and that of ubiquitin is 8.5 kDa, the lowest band in this blot is presumed as mono-ubiquitination, and the second and the third bands may represent GFP-SYP61 with di- and tri-ubiquitination. I also confirmed ubiquitination of SYP61 using the FLAG-tag fused SYP61 (FLAG-SYP61), and FLAG-GFP as a control (Fig. 11B). Based on their molecular weights, the bands detected with ubiquitin antibody were likely ubiquitinated SYP61, not GFP- or FLAG-tag or the other interactors. To further assess the biochemical characteristics of SYP61 ubiquitination, I analyzed the ubiquitin chain type. The second band of ubiquitinated SYP61, which is slightly lower than 75 kDa, was also bound by the antibody specific for K63-linked, but not K48-linked, ubiquitination (Fig. 11C). These findings revealed that SYP61 was ubiquitinated in plants, and that some pools of SYP61 are modified by K63-type ubiquitination.

ATL31 has an ability to mediate SYP61 ubiquitination

To examine the direct involvement of ATL31 in SYP61 ubiquitination, *in vitro*

ubiquitination assays were performed with MBP-tag fused ATL31 (MBP-ATL31) and GST-tag fused SYP61 (GST-SYP61) recombinant proteins. Incubation of GST-SYP61 with MBP-ATL31 for 1 or 3 hours, followed by immunoblotting with either anti-GST or anti-ubiquitin antibody, showed time-associated shifting of the GST-SYP61 bands (Fig. 12A). This ubiquitination signal was not detected after incubation with GST protein, indicating that SYP61 was ubiquitinated by ATL31 *in vitro*. The molecular size of the bands suggested that SYP61 was ubiquitinated with at least one molecule (mono-ubiquitin) but could also be ubiquitinated with two molecules. The two-ubiquitin-bound SYP61 was also detected with anti-K63 ubiquitination antibody (Fig. 12A), indicating that ATL31 can catalyze the attachment of a K63-linked ubiquitin chain to SYP61. As the upshifted bands of ubiquitinated GST-SYP61 were also observed with the ubiquitin protein without lysine 63 (Ub-K63R), ATL31 can also catalyze other types of ubiquitination, such as multiple-mono or other chain types (Fig. 13A). Nevertheless, the anti-K63 ubiquitination antibody did not detect the di-ubiquitination of GST-SYP61 with Ub-K63R, whereas the band was detected with the K63-only ubiquitin mutant, which can only form K63-linked chains, further confirming the existence of the K63-linked chain (Fig. 13A, B). Mass spectrometry showed that five lysine residues on SYP61, four on the SNARE domain, were ubiquitinated by ATL31 *in vitro* (Fig. 12B, Supplemental Table 3). I also confirmed that ATL31 ubiquitinates SYP61 in plant cells. GFP-SYP61 was expressed alone or with 3xFLAG tagged ATL31 (ATL31-3xFLAG) or ATL31^{C143S} (ATL31^{C143S}-3xFLAG) in *N. benthamiana* leaves by agroinfiltration. As a result, co-expression of ATL31-3xFLAG enhanced ubiquitination of SYP61 including K63-linked chain (Fig. 12C). This signal enhancement was not observed with the catalytically inactive form of ATL31, indicating

ATL31 enhanced SYP61 ubiquitination through its ubiquitination activity.

Ubiquitination of SYP61 is affected by C/N-nutrient availability

Finally, I investigated the relevance of SYP61 ubiquitination in the plant C/N-nutrient responses (Fig. 14A). To check the gradual effect of the C/N-nutrient condition, the Arabidopsis transgenic plants *pSYP61:GFP-SYP61* grown in liquid medium containing 100 mM Glc/30 mM N for 10 days were treated with 6 different medium containing 0, 100 or 200 mM Glc and 30 or 0.3 mM N for 3 hours. Interestingly, the signal of the ubiquitinated SYP61 was the highest in the 0 mM Glc/30 mM N treated sample. The difference of the signal of K63-linked chain was even more significant. The signal was higher in the 0 mM Glc treated samples than the other glucose conditions with the same nitrogen status. Comparing the two 0 mM Glc treated samples with different N conditions, the one with 30 mM N showed higher band intensity than the one with 0.3 mM N. The overall ubiquitination profiles did not show this tendency, suggesting SYP61 is specifically regulated (Fig. 14B). Because the ubiquitination signals of SYP61 were not decreased by the addition of the mannitol instead of glucose, it was confirmed that the observed difference was not due to the osmotic conditions (Fig. 14C). As the SYP61 ubiquitination was up-regulated in lower C/higher N condition, 0 mM Glc/60 mM N low C/high N condition was used in the following experiments. To test if ATL31 can mediate the low C/high N-induced SYP61 ubiquitination, we performed the experiment with Arabidopsis transgenic plants expressing mRFP-SYP61 in ATL31 overexpressor background (*pSYP61:mRFP-SYP61* in *2xp35S:ATL31-GFP*). The plants were grown in the liquid medium containing 100 mM Glc/30 mM N for 11 days, and treated with the low C/high N medium containing 0 mM Glc and 60 mM N for 0, 45, 90

or 180 minutes (Fig. 15). The total and the K63-linked ubiquitination of mRFP-SYP61 was the highest 45 minutes after the treatment, and gradually decreased in wild-type background. This tendency was the same in the ATL31 overexpressor background, but the amplitude was much higher. I also performed the experiment using the transgenic plants expressing GFP-SYP61 in the double knockout mutant of *ATL31* and the closest homologue *ATL6* (*pSYP61:GFP-SYP61* in *atl31-1/6-1*) to confirm their necessity (Fig. 16). However, SYP61 ubiquitination was not abolished in the mutant background, and responded to the C/N-nutrient treatment as in wild-type background. Thus, ATL31 is not an exclusive ubiquitin ligase in this process.

To test the possibility that the ubiquitination enhances the internalization of SYP61 from the plasma membrane, I quantified the amount of the mRFP-SYP61 in the plasma membrane using the plant materials and the C/N-nutrient conditions mentioned above (Fig. 17). As a result, the proportion of the plasma membrane-localized mRFP-SYP61 dropped accordingly to the lower C/higher N. However, the amount of the plasma membrane localized SYP61 was not decreased by ATL31 overexpression. Therefore, the ATL31-mediated ubiquitination of SYP61 is not likely serving as an endocytosis signal.

DISCUSSION

SNARE protein SYP61 is a mediator of post-Golgi membrane trafficking in Arabidopsis (Sanderfoot et al., 2001; Uemura et al., 2004). In this study, I identified SYP61 as an interactor of a ubiquitin ligase ATL31. My results suggested the cooperative function of SYP61 with ATL31, including proper traffic regulation of ATL31 by SYP61, is important for plant adaptations to disrupted high C/low N-nutrient stress conditions. Because SYP61 is a Qc-SNARE, the suppressed expression of SYP61

protein may have caused the low efficiency of membrane fusion at the TGN/EE and resulted in the dispersion of ATL31-GFP positive compartments.

I also found SYP61 is ubiquitinated with K63-linked chain in plant cells. Furthermore, low C/high N-nutrient condition enhances ubiquitination of SYP61, and ATL31 can promote this process. ATL31 catalyzes mono and K63-linked ubiquitination of SYP61 *in vitro* and in plant cells, although it is not an exclusive ubiquitin ligase. The ubiquitination of SYP61 detected in this study may contain multiple types with different molecular meanings. Firstly, the mass spectrometry analysis identified several sites of SYP61 directly ubiquitinated by ATL31 *in vitro*. In the *in planta* assays, while the ubiquitination bands of higher molecular weight than di-Ub bands were detected by the ubiquitination antibody, the bands were not clearly detected by the K63-chain specific antibody. Thus, the bands upper than di-Ub may contain SYP61 with non-K63-linked chain or multiple-mono-ubiquitination. These observations imply the heterogeneity of the ubiquitination of SYP61. Both the physiological and molecular functions of the SYP61 ubiquitination remain open questions, but there are a few things that can be discussed from my results here. Firstly, it is not likely ATL31 targets SYP61 to enhance plant growth under high C/low N-nutrient conditions, because these conditions down-regulated SYP61 ubiquitination. Secondly, the ATL31-mediated ubiquitination of SYP61 is not likely serving as an endocytosis signal, while the possibility that some batch of the low C/high N-mediated ubiquitination works in this pathway cannot be excluded. Because both ATL31 and SYP61 colocalize with the TGN/EE and the LE markers, it will be interesting to examine if the ATL31-mediated ubiquitination modifies the SYP61-mediated trafficking pathway on those compartments. A recent study reported the TGN/EE with SYP61 harbors both secretory-trafficking zone with an

R-SNARE VAMP721 and vacuolar-targeting zone with VAMP727 (Shimizu et al., 2021). In response to flg22 treatment, the proportion of the hybrid compartment of the TGN/EE and the LE marked by SYP61 and ARA7/RABF2b increases temporary to mediate endocytic trafficking of FLS2 (Choi et al., 2013). It is also reported that SYP61 localizes not only to the TGN/EE, but also to the plasma membrane and the vacuolar membranes under specific conditions (Gendre et al., 2013; Hachez et al., 2014; Rosquete et al., 2019; Heinze et al., 2020). This dynamic and seemingly undiscriminating behavior of SYP61 suggests as-yet-unknown post-translational mechanisms involved in the regulation of SYP61 localization and function in response to environmental stimuli, and ubiquitination may be involved in the process. There are not many reports on ubiquitination of SNARE proteins so far, but they have shown its involvement in several different molecular pathways. In yeast, ubiquitination of Tlg1, the SYP61 orthologue, and a Qa-SNARE Pep12 serves as a signal for vacuolar degradation through MVB (Reggiori and Pelham, 2002; Valdez-Taubas and Pelham, 2005). Poly-ubiquitination of a Rat Qa-SNARE Syntaxin1 induces its proteasomal degradation (Chin et al., 2002). On the other hand, mono-ubiquitination of a Qa-SNARE Syntaxin3 triggers non-degradative endocytosis in human epithelial cells (Giovannone et al., 2017). Also, K63-linked ubiquitination of Snc1, an yeast R-SNARE that mediates trafficking between the plasma membrane and the TGN, functions as non-degradative trafficking signal that facilitates its recycling back from the endocytic pathway to the exocytic pathway (Xu et al., 2017). In case of a human Qa-SNARE Syntaxin5, mono-ubiquitination and subsequent deubiquitination serve as a gate for the time-specific formation of SNARE complex to regulate Golgi membrane fusion during the cell cycle (Huang et al., 2016). In addition, K63-linked ubiquitination of a human

R-SNARE Sec22b is also implied to be involved in SNARE complex formation during interaction with a bacterial pathogen *Legionella pneumophila* (Kitao et al., 2020). In plants, there is a report that identified a plasma membrane localized Qa-SNARE SYP122 in a K63-linked ubiquitinome analysis in Arabidopsis (Johnson and Vert, 2016), although its molecular upstream and downstream effect have not been characterized. It seems SNARE ubiquitination functions as various molecular signals in a wide range of species. Future experiments including analysis of ubiquitination-defective mutant of SYP61 will reveal the detailed function of this post-translational modification.

The finding that ATL31 has multiple ubiquitination targets also suggested the multifunctionality of ATL31. In addition to this, our MS-based analysis shown in (Hasegawa et al., provisionally accepted) indicated that ATL31 has an ability to catalyze multiple ubiquitin chain types. Ubiquitination chain is formed by the attachment of ubiquitin (donor ubiquitin) onto the former ubiquitin (acceptor ubiquitin), and the ubiquitin chain type is directly determined by the positioning of the donor and the acceptor ubiquitin molecules (Deol et al., 2019). Therefore, in case the ubiquitination chain is formed onto the ubiquitin which is already bound to the target, all of the proteins in the complex in this process will serve as the determinants of the chain type. In case of a RING type ubiquitin ligase like ATL31, the major determinants will be E2, ubiquitin ligase itself, and the target proteins (Deol et al., 2019; Romero-Barrios et al., 2019). Arabidopsis genome codes 37 E2 genes (Callis, 1995), and the ubiquitin chain types mediated by ATL31 will be affected by which E2 protein it interacts with. It is also possible that other co-factors and the post-translational modification of ATL31 have effects on this process. As human UbcH5a was used as E2 in the *in vitro* assay here and the MS-based chain type analysis mentioned above, the ubiquitination types catalyzed

by ATL31 in plant cell needs further investigation. Nevertheless, the MS-based chain type analysis showed the potential of ATL31 to catalyze those multiple types of ubiquitination, and this suggested a possibility that ATL31 may mediate multiple cellular signals via ubiquitination of distinct target proteins. Previous studies reported that ATL31 targets 14-3-3 proteins for proteasomal degradation through the phosphorylation by CIPK7/12/14 kinases under high C/low N-nutrient stress conditions (Sato et al., 2011; Yasuda et al., 2014, 2017). Thus, the activity of ATL31, including the target interactions and possibly the type of ubiquitin linkages, seems to be tightly regulated in response to environmental conditions. The SYP61 ubiquitination by ATL31 might be also activated by as-yet-unknown upstream signals.

In addition to C/N-nutrient responses, ATL31 and SYP61 may interact in other environmental responses. Not only high C/low N-nutrient stress, ATL31 positively regulates plant resistance to pathogen attacks and possibly to salt stress (Maekawa et al., 2012, 2014; Peng et al., 2014; Wibowo et al., 2016). In plant immunity, ATL31 enhances callose deposition (Maekawa et al., 2012, 2014). ATL31 targeted to fungal penetration sites in association with SYP121/PEN1, and accelerated the formation of rigid cell walls called papillae (Maekawa et al., 2014), suggesting that ATL31 possibly mediates vesicle trafficking of cell wall material and/or the related enzymes. SYP61 is also reported to be involved in salt stress tolerances and cell wall secretion. The *osm1* mutant is hypersensitive to the salt and osmotic stresses (Zhu et al., 2002), and shows disrupted localization pattern of the plasma membrane aquaporin PIP2;7 (Hachez et al., 2014). Proteomics on SYP61 compartment has identified cell wall relating enzymes as potential cargos (Drakakaki et al., 2012), and recent advanced glycomic analysis reported that SYP61 also mediates trafficking of cell wall materials, such as

polysaccharides and glycoproteins (Wilkop et al., 2019). In addition to the overlap in the subcellular localization and the physical interaction, these functional similarities of ATL31 and SYP61 suggest their possible relevance in diverse physiological processes in plants.

This study demonstrated the importance of membrane traffic regulation by a SNARE protein in plant nutrient responses. In addition, it also suggested a possibility that SNARE proteins are regulated via ubiquitination in response to nutrient conditions. Future studies should reveal the downstream effect of the SNARE ubiquitination, as well as how common this modification is among SNARE proteins. It will also be interesting to find out further cargos whose localization is regulated in response to C/N-nutrient conditions. The findings in this research provided new insights into the membrane trafficking machinery and ubiquitin signaling in plant nutrient responses.

REFERENCES

Aoyama, S., Huarancca Reyes, T., Guglielminetti, L., Lu, Y., Morita, Y., Sato, T., and Yamaguchi, J. (2014a). Ubiquitin ligase ATL31 functions in leaf senescence in response to the balance between atmospheric CO2 and nitrogen availability in Arabidopsis. Plant Cell Physiol. **55**: 293–305.

Aoyama, S., Lu, Y., Yamaguchi, J., and Sato, T. (2014b). Regulation of senescence under elevated atmospheric CO_2 via ubiquitin modification. Plant Signal. Behav. **9**: e28839.

Barberon, M., Zelazny, E., Robert, S., Conéjéro, G., Curie, C., Friml, J., and Vert, G. (2011). Monoubiquitin-dependent endocytosis of the iron-regulated transporter 1 (IRT1) transporter controls iron uptake in plants. Proc. Natl. Acad. Sci. U. S. A. **108**: E450-8.

Callis, J. (1995). Regulation of Protein Degradation. Plant Cell **7**: 845–857.

Callis, J. (2014). The ubiquitination machinery of the ubiquitin system. Arab. B. **12**: e0174.

Chin, L.S., Vavalle, J.P., and Li, A. (2002). Staring, a novel E3 ubiquitin-protein ligase that targets syntaxin 1 for degradation. J. Biol. Chem. **277**: 35071–35079.

Choi, S., Tamaki, T., Ebine, K., Uemura, T., Ueda, T., and Nakano, A. (2013). RABA members act in distinct steps of subcellular trafficking of the FLAGELLIN SENSING2 receptor. Plant Cell **25**: 1174–87.

Coruzzi, G.M. and Zhou, L. (2001). Carbon and nitrogen sensing and signaling in plants: emerging “matrix effects”. Curr. Opin. Plant Biol. **4**: 247–53.

Deol, K.K., Lorenz, S., and Strieter, E.R. (2019). Enzymatic Logic of Ubiquitin Chain Assembly. Front. Physiol. **10**: 1–14.

Dettmer, J., Hong-Hermesdorf, A., Stierhof, Y.-D., and Schumacher, K. (2006). Vacuolar H+-ATPase activity is required for endocytic and secretory trafficking in Arabidopsis. Plant Cell **18**: 715–30.

Drakakaki, G., van de Ven, W., Pan, S., Miao, Y., Wang, J., Keinath, N.F., Weatherly, B., Jiang, L., Schumacher, K., Hicks, G., and Raikhel, N. (2012). Isolation and proteomic analysis of the SYP61 compartment reveal its role in exocytic trafficking in Arabidopsis. Cell Res. **22**: 413–24.

Dröse, S., Bindseil, K.U., Bowman, E.J., Siebers, A., Zeeck, A., and Altendorf, K. (1993). Inhibitory Effect of Modified Bafilomycins and Concanamycins on P- and V-Type Adenosinetriphosphatases. Biochemistry **32**: 3902–3906.

Dubeaux, G., Neveu, J., Zelazny, E., and Vert, G. (2018). Metal Sensing by the IRT1 Transporter-Receptor Orchestrates Its Own Degradation and Plant Metal Nutrition. Mol. Cell **69**: 953-964.e5.

Fecht-Bartenbach, J. Von Der, Bogner, M., Krebs, M., Stierhof, Y.-D., Schumacher, K., and Ludewig, U. (2007). Function of the anion transporter AtCLC-d in the trans-Golgi network. Plant J. **50**: 466–474.

Fujiwara, M., Uemura, T., Ebine, K., Nishimori, Y., Ueda, T., Nakano, A., Sato, M.H., and Fukao, Y. (2014). Interactomics of Qa-SNARE in arabidopsis thaliana. Plant Cell Physiol. **55**: 781–789.

Geldner, N., Anders, N., Wolters, H., Keicher, J., Kornberger, W., Muller, P., Delbarre, A., Ueda, T., Nakano, A., and Jürgens, G. (2003). The Arabidopsis GNOM ARF-GEF mediates endosomal recycling, auxin transport, and auxin-dependent plant growth. Cell **112**: 219–230.

Gendre, D., McFarlane, H.E., Johnson, E., Mouille, G., Sjödin, A., Oh, J.,

Levesque-Tremblay, G., Watanabe, Y., Samuels, L., and Bhalerao, R.P. (2013). Trans-Golgi network localized ECHIDNA/Ypt interacting protein complex is required for the secretion of cell wall polysaccharides in Arabidopsis. Plant Cell **25**: 2633–46.

Gilles, J.-F., Dos Santos, M., Boudier, T., Bolte, S., and Heck, N. (2017). DiAna, an ImageJ tool for object-based 3D co-localization and distance analysis. Methods **115**: 55–64.

Giovannone, A.J., Reales, E., Bhattaram, P., Fraile-Ramos, A., and Weimbs, T. (2017). Mono-ubiquitination of syntaxin 3 leads to retrieval from the basolateral plasma membrane and facilitates cargo recruitment to exosomes. Mol. Biol. Cell: 1–23.

Grebe, M., Xu, J., Möbius, W., Ueda, T., Nakano, A., Geuze, H.J., Rook, M.B., and Scheres, B. (2003). Arabidopsis sterol endocytosis involves actin-mediated trafficking via ARA6-positive early endosomes. Curr. Biol. **13**: 1378–87.

Hachez, C., Laloux, T., Reinhardt, H., Cavez, D., Degand, H., Grefen, C., De Rycke, R., Inzé, D., Blatt, M.R., Russinova, E., and Chaumont, F. (2014). Arabidopsis SNAREs SYP61 and SYP121 coordinate the trafficking of plasma membrane aquaporin PIP2;7 to modulate the cell membrane water permeability. Plant Cell **26**: 3132–47.

Heinze, L., Freimuth, N., Rößling, A., Hahnke, R., Riebschläger, S., Fröhlich, A., Sampathkumar, A., McFarlane, H.E., and Sauer, M. (2020). EPSIN1 and MTV1 define functionally overlapping but molecularly distinct trans -Golgi network subdomains in Arabidopsis. Proc. Natl. Acad. Sci. **117**: 25880–25889.

Hershko, A. and Ciechanover, A. (1998). The ubiquitin system. Annu. Rev. Biochem.

67: 425–79.

Huang, S., Tang, D., and Wang, Y. (2016). Monoubiquitination of Syntaxin 5 Regulates Golgi Membrane Dynamics during the Cell Cycle. Dev. Cell **38**: 73–85.

Huarancca Reyes, T., Scartazza, A., Pompeiano, A., Ciurli, A., Lu, Y., Guglielminetti, L., and Yamaguchi, J. (2018). Nitrate reductase modulation in response to changes in c/n balance and nitrogen source in arabidopsis. Plant Cell Physiol. **59**: 1248–1254.

Inada, N., Betsuyaku, S., Shimada, T.L., Ebine, K., Ito, E., Kutsuna, N., Hasezawa, S., Takano, Y., Fukuda, H., Nakano, A., and Ueda, T. (2016). Modulation of Plant RAB GTPase-Mediated Membrane Trafficking Pathway at the Interface Between Plants and Obligate Biotrophic Pathogens. Plant Cell Physiol. **57**: 1854–1864.

Isono, E. and Kalinowska, K. (2017). ESCRT-dependent degradation of ubiquitylated plasma membrane proteins in plants. Curr. Opin. Plant Biol. **40**: 49–55.

Jahn, R. and Scheller, R.H. (2006). SNAREs--engines for membrane fusion. Nat. Rev. Mol. Cell Biol. **7**: 631–43.

Jaillais, Y., Fobis-Loisy, I., Miège, C., and Gaude, T. (2008). Evidence for a sorting endosome in Arabidopsis root cells. Plant J. **53**: 237–247.

Johnson, A. and Vert, G. (2016). Unraveling K63 Polyubiquitination Networks by Sensor-Based Proteomics. Plant Physiol. **171**: 1808–20.

Kasai, K., Takano, J., Miwa, K., Toyoda, A., and Fujiwara, T. (2011). High boron-induced ubiquitination regulates vacuolar sorting of the BOR1 borate transporter in Arabidopsis thaliana. J. Biol. Chem. **286**: 6175–6183.

Kim, S.-J. and Bassham, D.C. (2011). TNO1 is involved in salt tolerance and vacuolar

trafficking in Arabidopsis. Plant Physiol. **156**: 514–26.

Kitao, T., Taguchi, K., Seto, S., Arasaki, K., Ando, H., Nagai, H., and Kubori, T. (2020). Legionella Manipulates Non-canonical SNARE Pairing Using a Bacterial Deubiquitinase. Cell Rep. **32**: 108107.

Korbei, B., Moulinier-Anzola, J., De-Araujo, L., Lucyshyn, D., Retzer, K., Khan, M.A., and Luschnig, C. (2013). Arabidopsis TOL proteins act as gatekeepers for vacuolar sorting of PIN2 plasma membrane protein. Curr. Biol. **23**: 2500–5.

Leitner, J., Petrasek, J., Tomanov, K., Retzer, K., Parezova, M., Korbei, B., Bachmair, a., Zazimalova, E., and Luschnig, C. (2012). Lysine63-linked ubiquitylation of PIN2 auxin carrier protein governs hormonally controlled adaptation of Arabidopsis root growth. Proc. Natl. Acad. Sci. **109**: 8322–8327.

Li, X. et al. (2020). Protein Phosphorylation Dynamics Under Carbon/Nitrogen-Nutrient Stress and Identification of a Cell Death-Related Receptor-Like Kinase in Arabidopsis. Front. Plant Sci. **11**: 1–15.

Lipka, V., Kwon, C., and Panstruga, R. (2007). SNARE-ware: the role of SNARE-domain proteins in plant biology. Annu. Rev. Cell Dev. Biol. **23**: 147–74.

Lu, Y., Yasuda, S., Li, X., Fukao, Y., Tohge, T., Fernie, A.R., Matsukura, C., Ezura, H., Sato, T., and Yamaguchi, J. (2016). Characterization of ubiquitin ligase SlATL31 and proteomic analysis of 14-3-3 targets in tomato fruit tissue (Solanum lycopersicum L.). J. Proteomics **143**: 254–264.

Ma, X. et al. (2020). Ligand-induced monoubiquitination of BIK1 regulates plant immunity. Nature: 1–5.

Maekawa, S., Inada, N., Yasuda, S., Fukao, Y., Fujiwara, M., Sato, T., and Yamaguchi, J. (2014). The Carbon/Nitrogen Regulator ARABIDOPSIS

TOXICOS EN LEVADURA31 Controls Papilla Formation in Response to Powdery Mildew Fungi Penetration by Interacting with SYNTAXIN OF PLANTS121 in Arabidopsis. Plant Physiol. **164**: 879–887.

Maekawa, S., Sato, T., Asada, Y., Yasuda, S., Yoshida, M., Chiba, Y., and Yamaguchi, J. (2012). The Arabidopsis ubiquitin ligases ATL31 and ATL6 control the defense response as well as the carbon/nitrogen response. Plant Mol. Biol. **79**: 217–227.

Martin, T., Oswald, O., and Graham, I.A. (2002). Arabidopsis seedling growth, storage lipid mobilization, and photosynthetic gene expression are regulated by carbon:nitrogen availability. Plant Physiol. **128**: 472–81.

Martins, S., Dohmann, E.M.N., Cayrel, A., Johnson, A., Fischer, W., Pojer, F., Satiat-Jeunemaître, B., Jaillais, Y., Chory, J., Geldner, N., and Vert, G. (2015). Internalization and vacuolar targeting of the brassinosteroid hormone receptor BRI1 are regulated by ubiquitination. Nat. Commun. **6**: 6151.

Matsuoka, K., Higuchi, T., Maeshima, M., and Nakamura, K. (1997). A Vacuolar-Type H+-ATPase in a Nonvacuolar Organelle Is Required for the Sorting of Soluble Vacuolar Protein Precursors in Tobacco Cells. Plant Cell **9**: 533–546.

Nakagawa, T., Kurose, T., Hino, T., Tanaka, K., Kawamukai, M., Niwa, Y., Toyooka, K., Matsuoka, K., Jinbo, T., and Kimura, T. (2007). Development of series of gateway binary vectors, pGWBs, for realizing efficient construction of fusion genes for plant transformation. J. Biosci. Bioeng. **104**: 34–41.

Obrdlik, P. et al. (2004). K+ channel interactions detected by a genetic system optimized for systematic studies of membrane protein interactions. Proc. Natl. Acad. Sci. U. S. A. **101**: 12242–7.

Oh, E., Akopian, D., and Rape, M. (2018). Principles of Ubiquitin-Dependent Signaling. Annu. Rev. Cell Dev. Biol. **34**: 137–162.

Peng, J., Li, Z., Wen, X., Li, W., Shi, H., Yang, L., Zhu, H., and Guo, H. (2014). Salt-Induced Stabilization of EIN3/EIL1 Confers Salinity Tolerance by Deterring ROS Accumulation in Arabidopsis. PLoS Genet. **10**: e1004664.

Pratelli, R., Sutter, J.U., and Blatt, M.R. (2004). A new catch in the SNARE. Trends Plant Sci. **9**: 187–195.

Reggiori, F. and Pelham, H.R.B. (2002). A transmembrane ubiquitin ligase required to sort membrane proteins into multivesicular bodies. Nat. Cell Biol. **4**: 117–123.

Robinson, D.G., Jiang, L., and Schumacher, K. (2008). The endosomal system of plants: charting new and familiar territories. Plant Physiol. **147**: 1482–92.

Romero-Barrios, N., Monachello, D., Dolde, U., Wong, A., San Clemente, H., Cayrel, A., Johnson, A., Lurin, C., and Vert, G. (2019). Advanced Cataloging of Lysine-63 Polyubiquitin Networks by Genomic, Interactome, and Sensor-based Proteomic Analyses. Plant Cell **32**: tpc.00568.2019.

Romero-Barrios, N. and Vert, G. (2018). Proteasome-independent functions of lysine-63 polyubiquitination in plants. New Phytol. **217**: 995–1011.

Rosquete, M.R., Worden, N., Ren, G., Sinclair, R.M., Pfleger, S., Salemi, M., Phinney, B.S., Domozych, D., Wilkop, T., and Drakakaki, G. (2019). AtTRAPPC11/ROG2: A Role for TRAPPs in Maintenance of the Plant Trans-Golgi Network/Early Endosome Organization and Function. Plant Cell **31**: 1879–1898.

Sanderfoot, A. (2007). Increases in the number of SNARE genes parallels the rise of multicellularity among the green plants. Plant Physiol. **144**: 6–17.

Sanderfoot, A.A., Assaad, F.F., and Raikhel, N. V (2000). The Arabidopsis genome. An abundance of soluble N-ethylmaleimide-sensitive factor adaptor protein receptors. Plant Physiol. **124**: 1558–69.

Sanderfoot, A.A., Kovaleva, V., Bassham, D.C., and Raikhel, N. V. (2001). Interactions between syntaxins identify at least five SNARE complexes within the Golgi/prevacuolar system of the Arabidopsis cell. Mol. Biol. Cell **12**: 3733–43.

Sato, T. et al. (2009). CNI1/ATL31, a RING-type ubiquitin ligase that functions in the carbon/nitrogen response for growth phase transition in Arabidopsis seedlings. Plant J. **60**: 852–64.

Sato, T., Maekawa, S., Yasuda, S., Domeki, Y., Sueyoshi, K., Fujiwara, M., Fukao, Y., Goto, D.B., and Yamaguchi, J. (2011). Identification of 14-3-3 proteins as a target of ATL31 ubiquitin ligase, a regulator of the C/N response in Arabidopsis. Plant J. **68**: 137–46.

Shimizu, Y. et al. (2021). Cargo sorting zones in the trans-Golgi network visualized by super-resolution confocal live imaging microscopy in plants. Nat. Commun. **12**: 1901.

Takeda, A., Sugiyama, K., Nagano, H., Mori, M., Kaido, M., Mise, K., Tsuda, S., and Okuno, T. (2002). Identification of a novel RNA silencing suppressor, NSs protein of Tomato spotted wilt virus. FEBS Lett. **532**: 75–9.

Tamura, K., Shimada, T., Ono, E., Tanaka, Y., Nagatani, A., Higashi, S.-I., Watanabe, M., Nishimura, M., and Hara-Nishimura, I. (2003). Why green fluorescent fusion proteins have not been observed in the vacuoles of higher plants. Plant J. **35**: 545–555.

Uemura, T., Nakano, R.T., Takagi, J., Wang, Y., Kramer, K., Finkemeier, I.,

Nakagami, H., Tsuda, K., Ueda, T., Schulze-Lefert, P., and Nakano, A. (2019). A Golgi-Released Subpopulation of the Trans-Golgi Network Mediates Protein Secretion in Arabidopsis. Plant Physiol. **179**: 519–532.

Uemura, T., Suda, Y., Ueda, T., and Nakano, A. (2014). Dynamic behavior of the trans-golgi network in root tissues of arabidopsis revealed by super-resolution live imaging. Plant Cell Physiol. **55**: 694–703.

Uemura, T., Ueda, T., and Nakano, A. (2012). The physiological role of SYP4 in the salinity and osmotic stress tolerances. Plant Signal. Behav. **7**: 1118–20.

Uemura, T., Ueda, T., Ohniwa, R.L., Nakano, A., Takeyasu, K., and Sato, M.H. (2004). Systematic Analysis of SNARE Molecules in *Arabidopsis*: Dissection of the post-Golgi Network in Plant Cells. Cell Struct. Funct. **29**: 49–65.

Valdez-Taubas, J. and Pelham, H. (2005). Swf1-dependent palmitoylation of the SNARE Tlg1 prevents its ubiquitination and degradation. EMBO J. **24**: 2524–2532.

Wang, J., Cai, Y., Miao, Y., Lam, S.K., and Jiang, L. (2009). Wortmannin induces homotypic fusion of plant prevacuolar compartments. J. Exp. Bot. **60**: 3075–3083.

Wibowo, A., Becker, C., Marconi, G., Durr, J., Price, J., Hagmann, J., Papareddy, R., Putra, H., Kageyama, J., Becker, J., Weigel, D., and Gutierrez-Marcos, J. (2016). Hyperosmotic stress memory in Arabidopsis is mediated by distinct epigenetically labile sites in the genome and is restricted in the male germline by DNA glycosylase activity. Elife **5**: 1–27.

Wickner, W. and Schekman, R. (2008). Membrane fusion. Nat. Struct. Mol. Biol. **15**: 658–64.

Wilkop, T., Pattathil, S., Ren, G., Davis, D.J., Bao, W., Duan, D., Peralta, A.G.,

Domozych, D.S., Hahn, M.G., and Drakakaki, G. (2019). A Hybrid Approach Enabling Large-Scale Glycomic Analysis of Post-Golgi Vesicles Reveals a Transport Route for Polysaccharides. Plant Cell **31**: 627–644.

Xu, P., Hankins, H.M., MacDonald, C., Erlinger, S.J., Frazier, M.N., Diab, N.S., Piper, R.C., Jackson, L.P., MacGurn, J.A., and Graham, T.R. (2017). COPI mediates recycling of an exocytic SNARE by recognition of a ubiquitin sorting signal. Elife **6**: 1–22.

Yamada, K., Yamashita-Yamada, M., Hirase, T., Fujiwara, T., Tsuda, K., Hiruma, K., and Saijo, Y. (2016). Danger peptide receptor signaling in plants ensures basal immunity upon pathogen-induced depletion of BAK1. EMBO J. **35**: 46–61.

Yasuda, S., Aoyama, S., Hasegawa, Y., Sato, T., and Yamaguchi, J. (2017). Arabidopsis CBL-Interacting Protein Kinases Regulate Carbon/Nitrogen-Nutrient Response by Phosphorylating Ubiquitin Ligase ATL31. Mol. Plant **10**: 605–618.

Yasuda, S., Sato, T., Maekawa, S., Aoyama, S., Fukao, Y., and Yamaguchi, J. (2014). Phosphorylation of Arabidopsis ubiquitin ligase ATL31 is critical for plant carbon/nitrogen nutrient balance response and controls the stability of 14-3-3 proteins. J. Biol. Chem. **289**: 15179–93.

Yoshinari, A., Hosokawa, T., Beier, M.P., Oshima, K., Ogino, Y., Hori, C., Takasuka, T.E., Fukao, Y., Fujiwara, T., and Takano, J. (2020). Transport-coupled ubiquitination of the borate transporter BOR1 for its boron-dependent degradation. Plant Cell: 1–19.

Zhai, Z., Keereetaweep, J., Liu, H., Feil, R., Lunn, J.E., and Shanklin, J. (2018). Trehalose 6-Phosphate Positively Regulates Fatty Acid Synthesis by Stabilizing WRINKLED1. Plant Cell **30**: 2616–2627.

Zhou, J. et al. (2018). Regulation of Arabidopsis brassinosteroid receptor BRI1 endocytosis and degradation by plant U-box PUB12/PUB13-mediated ubiquitination. Proc. Natl. Acad. Sci. U. S. A. **115**: E1906–E1915.

Zhu, J., Gong, Z., Zhang, C., Song, C., Damsz, B., Inan, G., Koiwa, H., Zhu, J., Hasegawa, P.M., and Bressan, R. a (2002). OSM1/SYP61: a syntaxin protein in Arabidopsis controls abscisic acid-mediated and non-abscisic acid-mediated responses to abiotic stress. Plant Cell **14**: 3009–28.

Zouhar, J., Rojo, E., and Bassham, D.C. (2009). AtVPS45 is a positive regulator of the SYP41/SYP61/VTI12 SNARE complex involved in trafficking of vacuolar cargo. Plant Physiol. **149**: 1668–78.

FIGURES AND LEGENDS

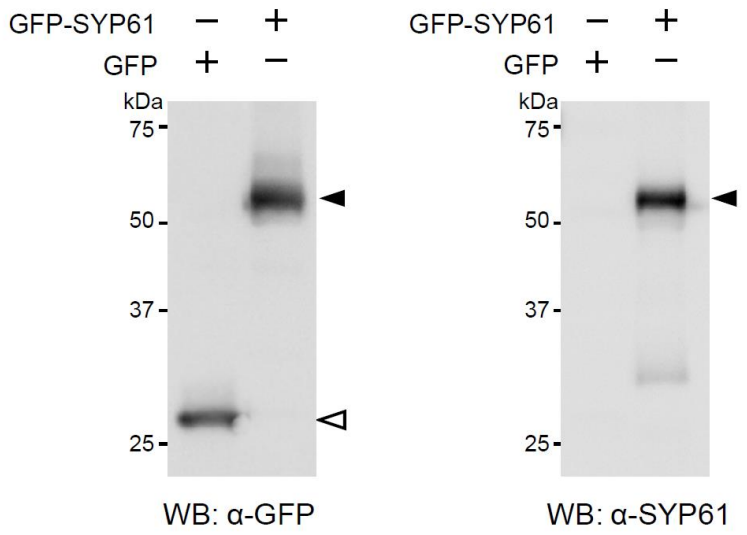
GFP-SYP61 − +
GFP + −
kDa
75
50
37
25
WB: α-GFP
GFP-SYP61 − +
GFP + −
kDa
75
50
37
25
WB: α-SYP61

Fig. 1

Fig. 1 Recognition of SYP61 protein by anti-SYP61 antibody.

Proteins were extracted from *N. benthamiana* leaves transiently expressing GFP (27 kDa) or GFP-SYP61 (56 kDa), and detected with anti-GFP and anti-SYP61 antibodies. The same amount of proteins were applied. Closed arrowheads indicate GFP-SYP61, and open arrowhead indicates GFP.

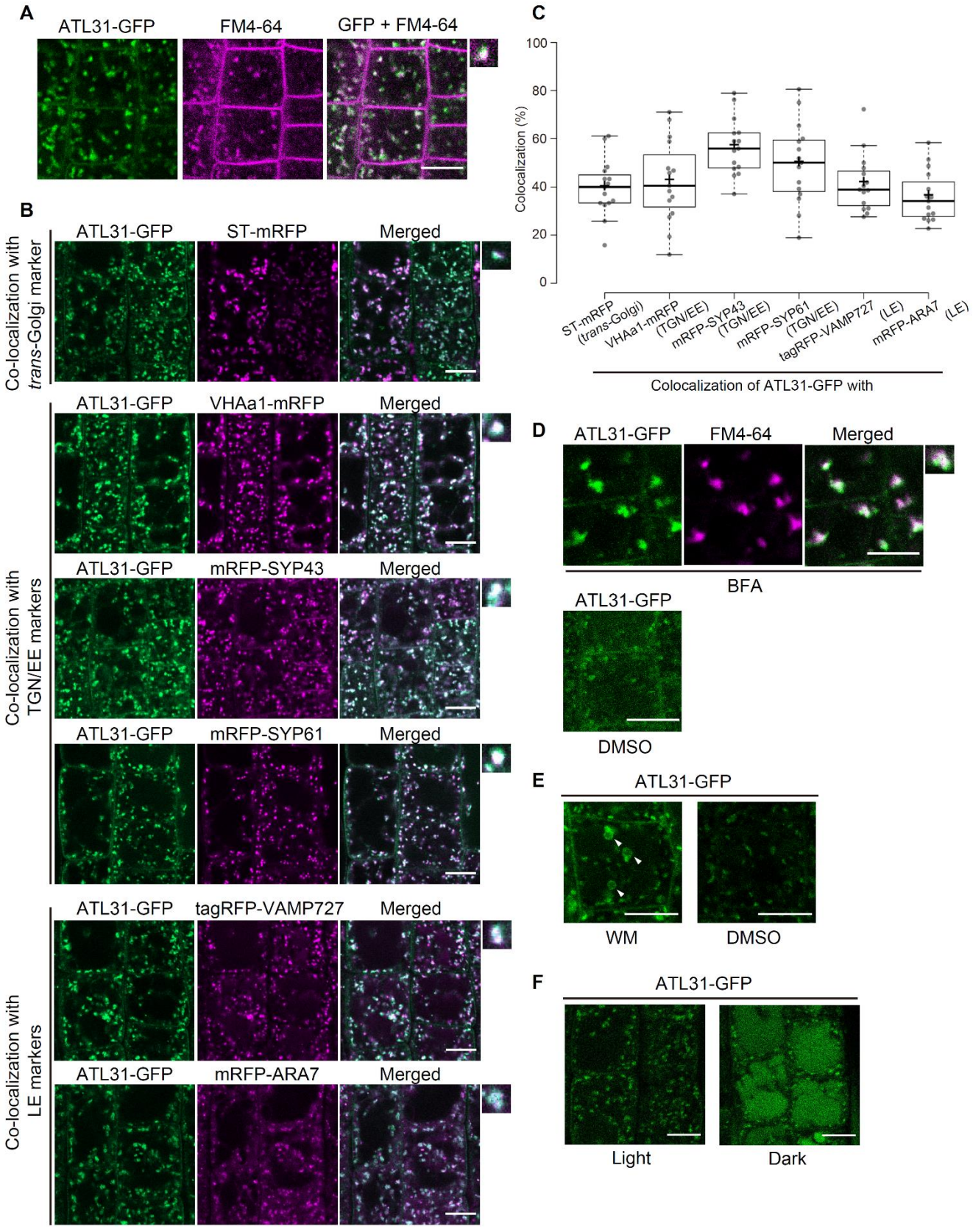
A
ATL31-GFP
FM4-64
GFP + FM4-64
B
Co-localization with trans-Golgi marker
ATL31-GFP
ST-mRFP
Merged
Co-localization with TGN/EE markers
ATL31-GFP
VHAa1-mRFP
Merged
ATL31-GFP
mRFP-SYP43
Merged
ATL31-GFP
mRFP-SYP61
Merged
Co-localization with LE markers
ATL31-GFP
tagRFP-VAMP727
Merged
ATL31-GFP
mRFP-ARA7
Merged
C
Colocalization (%)
100
80
60
40
20
0
ST-mRFP (trans-Golgi)
VHAa1-mRFP (TGN/EE)
mRFP-SYP43 (TGN/EE)
mRFP-SYP61 (TGN/EE)
tagRFP-VAMP727 (LE)
mRFP-ARA7 (LE)
Colocalization of ATL31-GFP with
D
ATL31-GFP
FM4-64
Merged
BFA
ATL31-GFP
DMSO
E
ATL31-GFP
WM
DMSO
F
ATL31-GFP
Light
Dark

Fig. 2

Fig. 2 ATL31 localizes to the plasma membrane and endosomal compartments.

(A) Representative confocal images of FM4-64 stained Arabidopsis root epidermal cells expressing ATL31-GFP. The root was stained with 2 μM FM4-64 for 2 minutes and washed with the medium without dye. The picture was taken 18 minutes after the staining. Bar = 10 μm.

(B) Representative confocal images of Arabidopsis root epidermal cells co-expressing ATL31-GFP with ST-mRFP (*trans*-Golgi), mRFP-SYP43 (TGN/EE), mRFP-SYP61 (TGN/EE), VHAa1-mRFP (TGN/EE), mRFP-ARA7 (LE), and tagRFP-VAMP727 (LE) (F1 generation). Right panels show enlarged view of the dot-like structures. LE, late endosome. Bars = 10 μm.

(C) Quantification of B. Percentage of the dot-like structures of ATL31-GFP colocalizing with the indicated markers were plotted. The center-center distance of the nearest dot-like structures were calculated by an ImageJ plugin DiAna, and the endosomes with distance closer than 0.2 μm (approximate theoretical resolution limit of the confocal microscope) were considered as colocalizing. n = 15 cell slices from 5 roots were analyzed. Box plots definition: center line, median; box limits, lower and upper quartiles; +, mean; dots, individual data points; whiskers, highest and lowest data points (The whiskers extend to data points that are less than 1.5 x IQR away from 1st/3rd quartile).

(D) Representative confocal images of Arabidopsis root epidermal cells expressing ATL31-GFP treated with 50 μM Brefeldin A (BFA) or DMSO for 30 minutes. Cells were stained with 5 μM FM4-64 15 minutes before BFA treatment. Right panels show enlarged view of the BFA bodies. Bars = 10 μm.

(E) Representative confocal images of Arabidopsis root epidermal cells expressing

ATL31-GFP treated with 33 μM Wortmannin (WM) or DMSO for 1 hour. Arrowheads indicate the ring like structures representing the vacuolized late endosomal compartments. Bars = 10 μm.

(F) Representative confocal images of Arabidopsis root epidermal cells expressing ATL31-GFP after light or dark treatment for 18 hours. Bars = 10 μm.

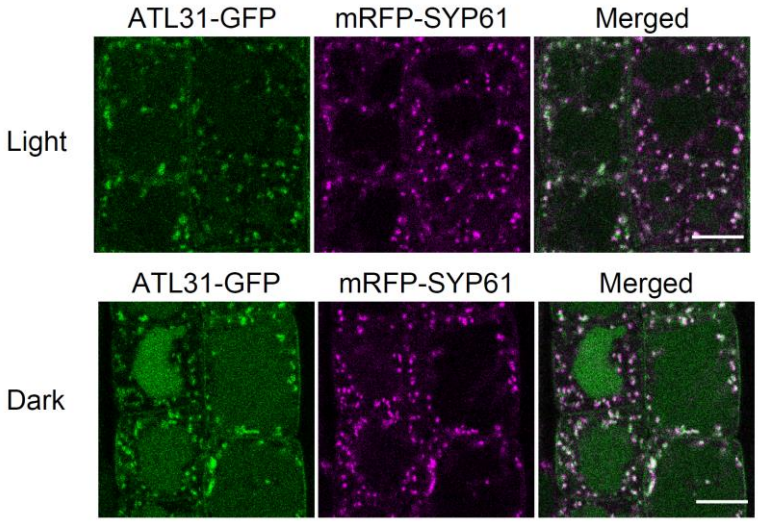
ATL31-GFP
mRFP-SYP61
Merged
Light
ATL31-GFP
mRFP-SYP61
Merged
Dark

Fig. 3

Fig. 3 ATL31-GFP was accumulated in the vacuole after 18-hr dark treatment, whereas mRFP-SYP61 was not.

Representative confocal images of Arabidopsis root cells co-expressing ATL31-GFP with mRFP-SYP61 (TGN/EE) (F1 generation) after light or dark treatment for 18 hours. Bars = 10 μm.

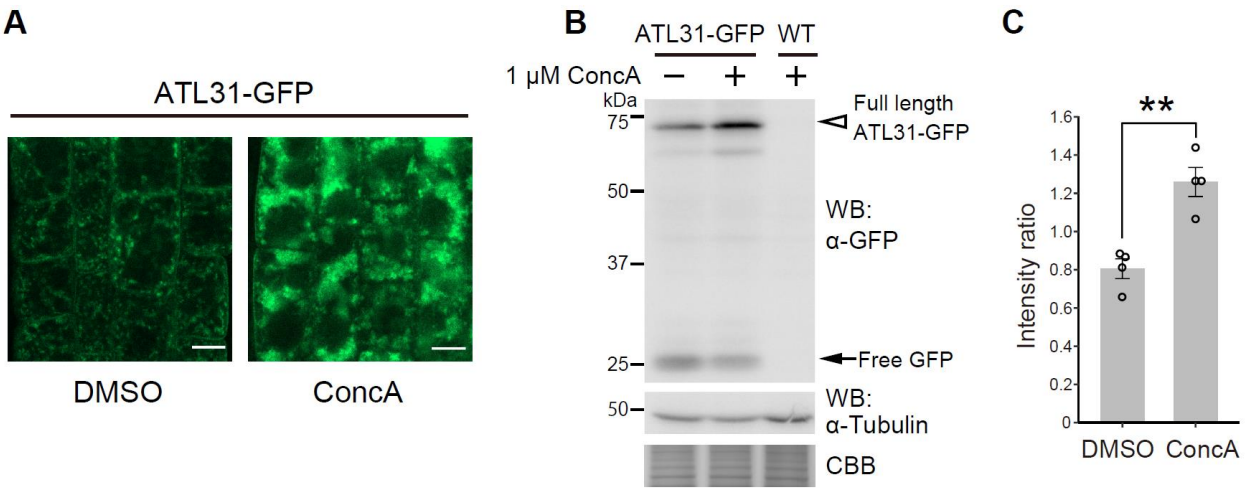
A
ATL31-GFP
DMSO
ConcA
B
ATL31-GFP
WT
1 μM ConcA
–
+
+
kDa
75
50
37
25
50
Full length
ATL31-GFP
WB:
α-GFP
Free GFP
WB:
α-Tubulin
CBB
C
**
Intensity ratio
1.6
1.4
1.2
1.0
0.8
0.6
0.4
0.2
0
DMSO
ConcA

Fig. 4

Fig. 4. ATL31-GFP is sensitive to Concanamycin A.

(A) Representative confocal images of Arabidopsis root epidermal cells expressing ATL31-GFP after 3 hours treatment of 1 μM Concanamycin A (ConcA) or DMSO (mock). Bars = 10 μm.

(B) Western blotting analysis after ConcA treatment. Arabidopsis plants expressing ATL31-GFP were incubated with 1 μM ConcA or DMSO for 3 hours. Immunoblot was performed with anti-GFP and anti-Tubulin (loading control) antibodies. Open arrowhead, ATL31-GFP (71 kDa); arrow, free GFP (about 27 kDa). CBB staining is shown as a loading control.

(C) Quantification of the western blotting analysis shown in (B). The ratio between the band intensity of full length ATL31-GFP and degraded free GFP was calculated. Data are means ± s.e.m. (n = 4 independent batches of plants). Statistical significance was determined by two-tailed Welch's *t*-test. (**P<0.01).

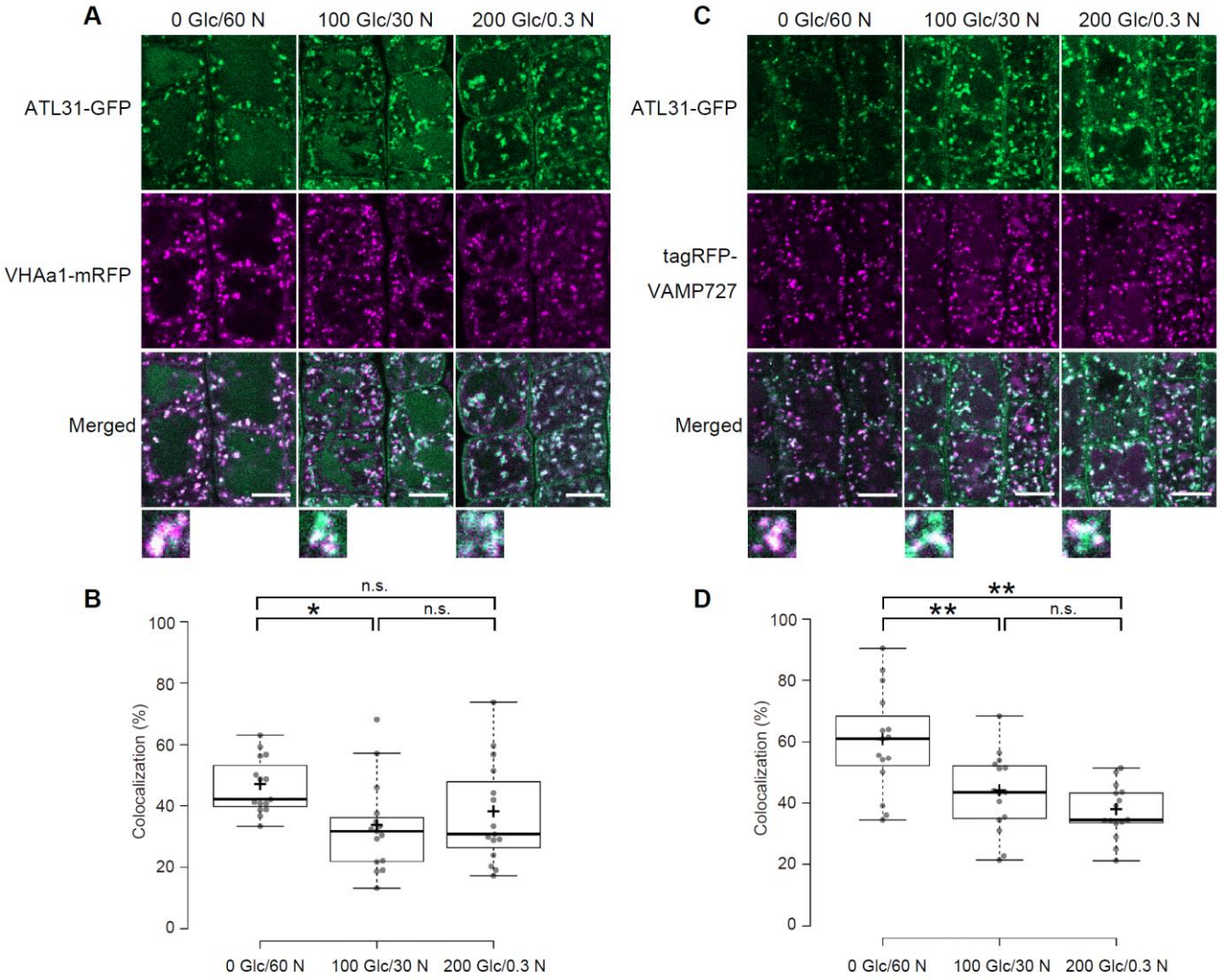
A
0 Glc/60 N
100 Glc/30 N
200 Glc/0.3 N
ATL31-GFP
VHAa1-mRFP
Merged
C
0 Glc/60 N
100 Glc/30 N
200 Glc/0.3 N
ATL31-GFP
tagRFP-
VAMP727
Merged
B
n.s.
*
n.s.
Colocalization (%)
100
80
60
40
20
0
0 Glc/60 N
100 Glc/30 N
200 Glc/0.3 N
D
**
**
n.s.
Colocalization (%)
100
80
60
40
20
0
0 Glc/60 N
100 Glc/30 N
200 Glc/0.3 N

Fig. 5

Fig. 5 Subcellular localization of ATL31 in response to C/N-nutrient conditions.

(A, C) Representative confocal images of Arabidopsis root epidermal cells co-expressing ATL31-GFP with VHAa1-mRFP (TGN/EE marker) (**A**) or tagRFP-VAMP727 (LE marker) (**C**). 6 days-grown plants were treated with liquid MS medium containing 0 mM glucose/60 mM nitrogen, 100 mM glucose/30 mM nitrogen or 200 mM glucose/0.3 mM nitrogen, and pictures were taken 90-110 minutes after the treatment. Bars = 10 μm.

(B, D) Percentage of the dot-like structures of ATL31-GFP colocalizing with VHAa1-mRFP (**B**) or tagRFP-VAMP727 (**D**) were plotted. The center-center distance of the nearest dot-like structures was calculated by an ImageJ plugin DiAna, and the endosomes with distance closer than 0.2 μm (approximate theoretical resolution limit of the confocal microscope) were considered as colocalizing. Box plots definition: center line, median; box limits, lower and upper quartiles; dots, individual data points; whiskers, highest and lowest data points (The whiskers extend to data points that are less than 1.5 x IQR away from 1st/3rd quartile). n = 15 cell slices from 5 roots were analyzed. Statistical differences were inferred by analysis of variance (ANOVA) followed by Tukey´s honestly significant difference (HSD) test (n.s., $P>0.05$; *$P<0.05$; **$P<0.01$).

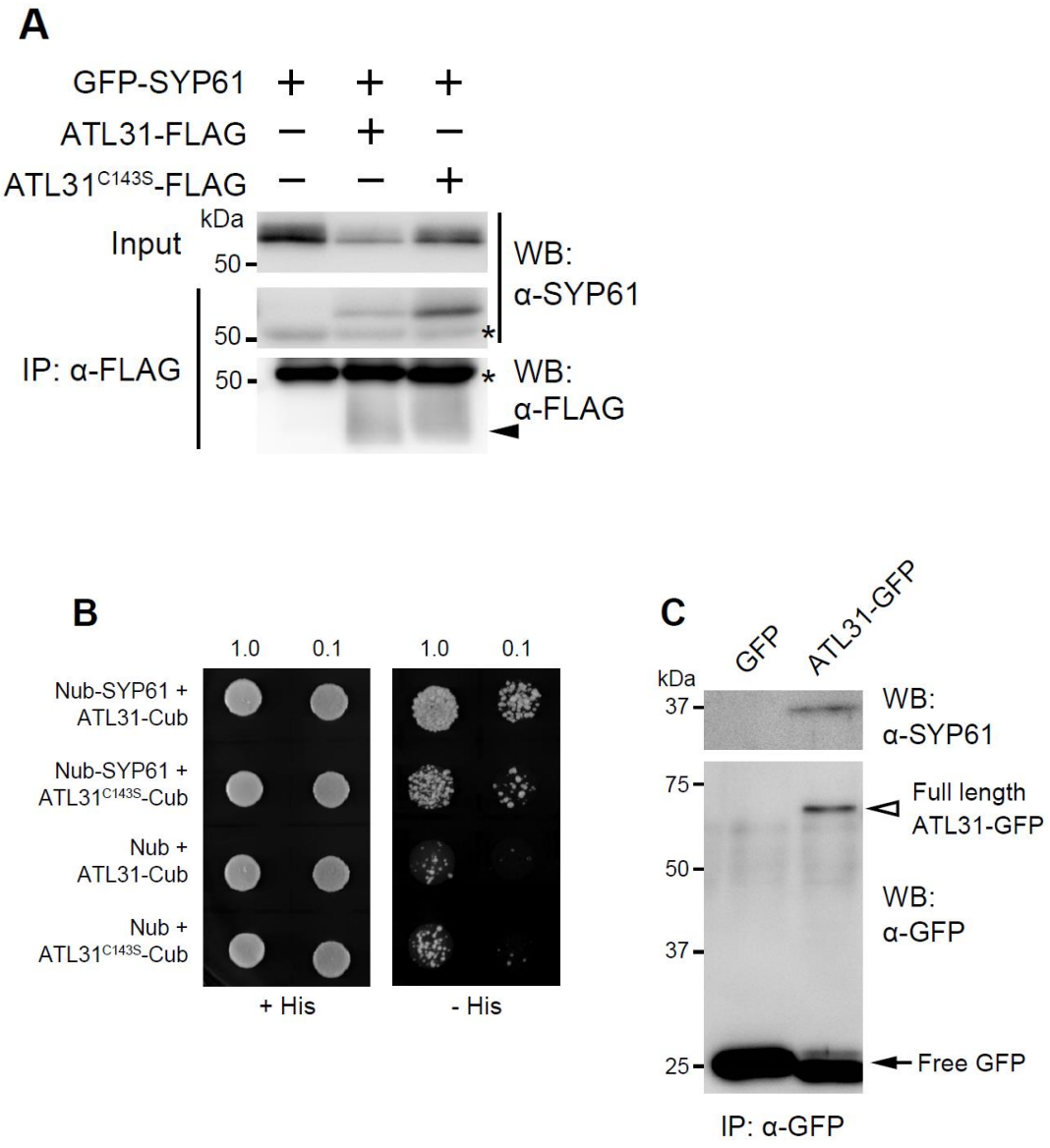
A
GFP-SYP61 + + +
ATL31-FLAG − + −
ATL31C143S-FLAG − − +
kDa
Input
50
WB:
α-SYP61
50
*
IP: α-FLAG
50
*
WB:
α-FLAG
B
1.0
0.1
1.0
0.1
Nub-SYP61 +
ATL31-Cub
Nub-SYP61 +
ATL31C143S-Cub
Nub +
ATL31-Cub
Nub +
ATL31C143S-Cub
+ His
- His
C
GFP
ATL31-GFP
kDa
37
WB:
α-SYP61
75
50
37
Full length
ATL31-GFP
WB:
α-GFP
25
Free GFP
IP: α-GFP

Fig. 6

Fig. 6 ATL31 interacts with SYP61.

(A) Co-immunoprecipitation of GFP-SYP61 (56 kDa) with ATL31-FLAG or ATL31$_{C143S}$-FLAG (43 kDa, indicated by arrowhead). Proteins were expressed in *N. benthamiana* leaves, and immunoprecipitated with anti-FLAG antibody beads, followed by immunoblotting with anti-SYP61 and anti-FLAG antibodies. Asterisks, nonspesific bands and IgG heavy chain.

(B) Split ubiquitin yeast-two hybrid assays of ATL31-Cub and ATL31$_{C143S}$-Cub with Nub-SYP61 or empty vector. Yeast cultures were diluted to 1 or 10 times (indicated 1.0 or 0.1 each), and grown on solid medium with or without histidine (His). Cub, C-terminal half of ubiquitin; Nub, N-terminal half of ubiquitin.

(C) Co-immunoprecipitation of endogenous SYP61 with ATL31-GFP in Arabidopsis. Proteins were extracted from Arabidopsis plants expressing GFP (27 kDa, indicated by arrow) or ATL31-GFP (71 kDa, indicated by open arrowhead), and subjected to immunoprecipitation with anti-GFP antibody beads, followed by immunoblotting with anti-SYP61 and anti-GFP antibodies.

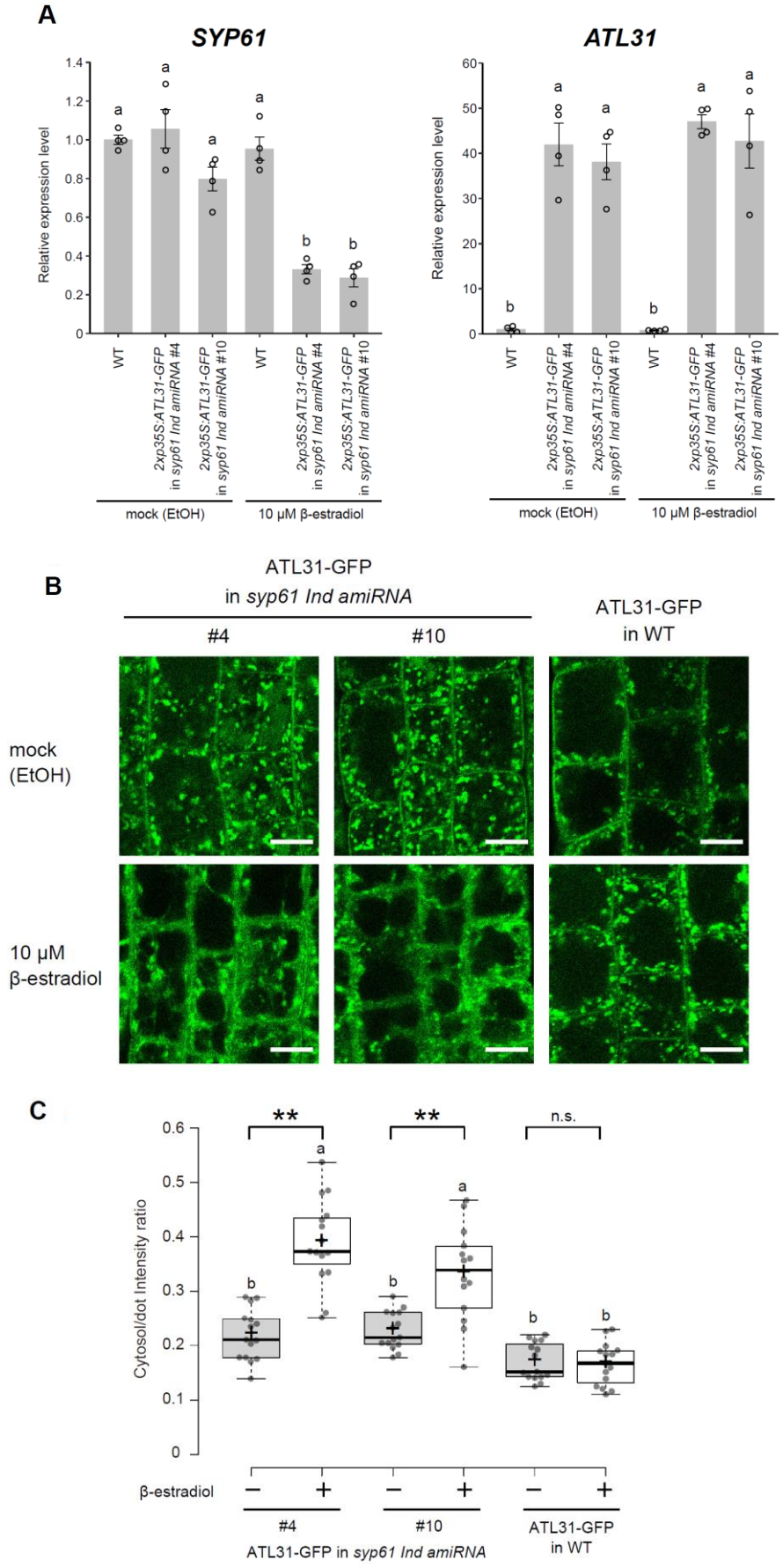
A
SYP61
ATL31
Relative expression level
WT
2xp35S:ATL31-GFP in syp61 Ind amiRNA #4
2xp35S:ATL31-GFP in syp61 Ind amiRNA #10
mock (EtOH)
10 μM β-estradiol
B
ATL31-GFP in syp61 Ind amiRNA
#4
#10
ATL31-GFP in WT
mock (EtOH)
10 μM β-estradiol
C
Cytosol/dot Intensity ratio
**
n.s.
β-estradiol
ATL31-GFP in syp61 Ind amiRNA
ATL31-GFP in WT

Fig. 7

Fig. 7 Subcellular localization of ATL31 was affected by induced knockdown of *SYP61*.

(A) Relative expression levels of of *SYP61* and *ATL31* mRNA transcript normalized by *18S rRNA*. Total RNA was extracted from wild-type (WT, Col-0) and F1 plants of *ATL31* overexpressor (*2xp35S:ATL31-GFP*) and *syp61* inducible knockdown lines (*syp61 Ind amiRNA* #4 and #10) grown for 16 days on 100 mM glucose/30 mM nitrogen with ethanol or 10 μM β-estradiol. Data are means ± s.e.m (n = 4 plants). Statistical differences were inferred by analysis of variance (ANOVA) followed by Tukey's honestly significant difference (HSD) test. Different letters are indicating significant difference (P<0.05).

(B) Representative confocal images of Arabidopsis root epidermal cells expressing ATL31-GFP in *syp61* inducible knockdown mutant (*syp61 Ind amiRNA*) (F3 generation, homo) or in wildtype (WT) background. Plants were grown for 7 days on medium containg ethanol (EtOH) or 10 μM β-estradiol. Bars = 10 μm. The induction of *SYP61* knockdown by β-estradiol in the used lines is confirmed in (**A**).

(C) Quantification of the intensity ratio of ATL31-GFP in the cytosol and the dot-like structures. The intracellular region excluding the dot-like structures was considered as "cytosol" here. n = 14-15 cell slices from 5 roots were analyzed. **P<0.01 by two-tailed Welch´s *t*-test. n.s., not significant. Different characters are showing significant difference defined by post-hoc Tukey HSD Test (P<0.05). Box plots definition: center line, median; box limits, lower and upper quartiles; +, mean; dots, individual data points; whiskers, highest and lowest data points (The whiskers extend to data points that are less than 1.5 x IQR away from 1st/3rd quartile).

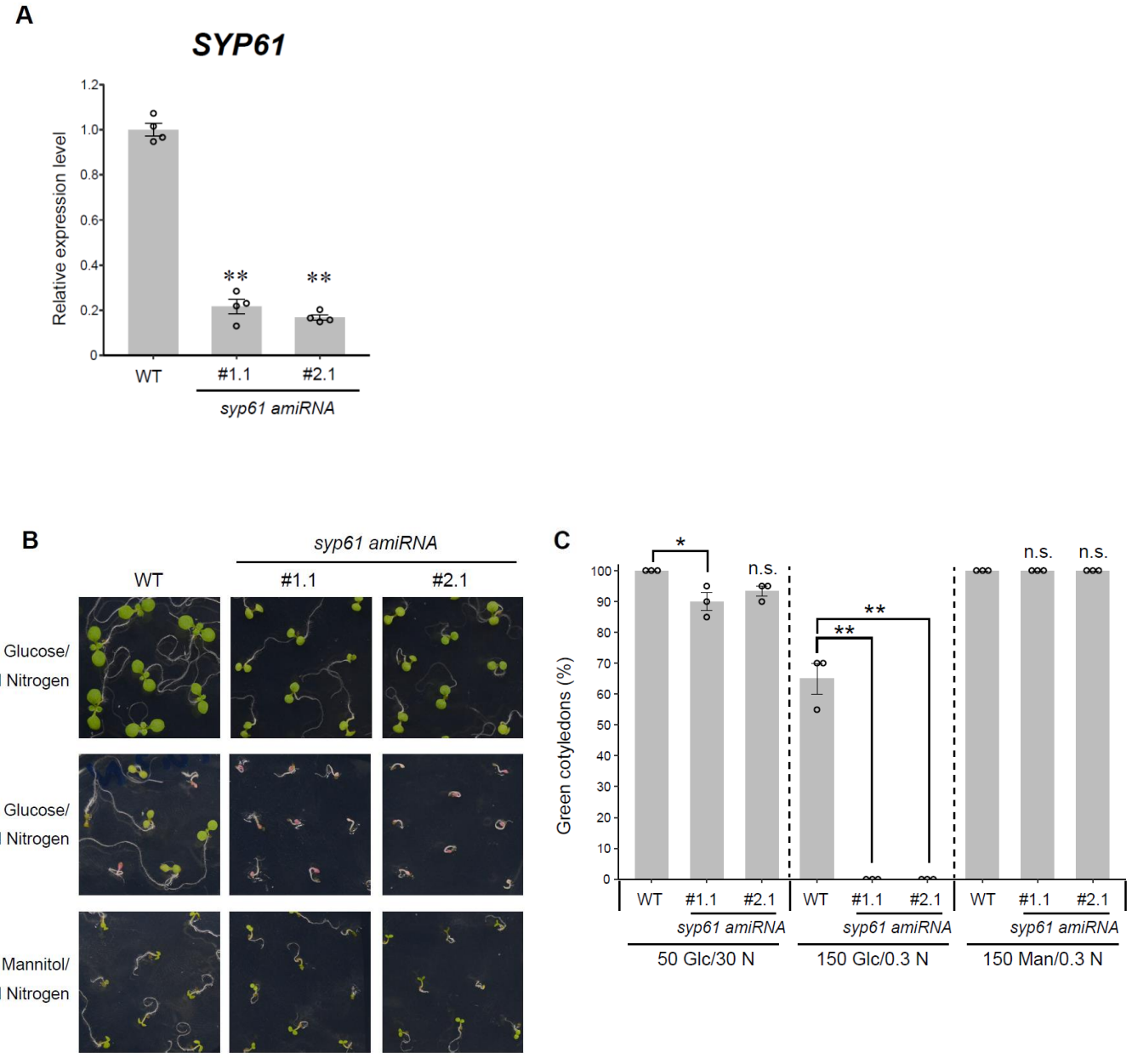
A
SYP61
Relative expression level
1.2
1.0
0.8
0.6
0.4
0.2
0
**
**
WT
#1.1
#2.1
syp61 amiRNA
B
syp61 amiRNA
WT
#1.1
#2.1
50 mM Glucose/
30 mM Nitrogen
150 mM Glucose/
0.3 mM Nitrogen
150 mM Mannitol/
0.3 mM Nitrogen
C
Green cotyledons (%)
100
90
80
70
60
50
40
30
20
10
0
*
n.s.
**
**
n.s.
n.s.
WT
#1.1
#2.1
syp61 amiRNA
50 Glc/30 N
150 Glc/0.3 N
150 Man/0.3 N

Fig. 8

Fig. 8 *syp61* knockdown mutants are hypersensitive to C/N-nutrient stress.

C/N-nutrient responses during post-germination growth.

(A) Relative expression levels of of *SYP61* mRNA transcript normalized by *18S rRNA*. Total RNA was extracted from WT (Col-0) and *syp61* constitutive knockdown mutant (*syp61 amiRNA*) seedlings grown for 7 days. Data are means ± s.e.m (n = 4 independent batches of plants). Asterisks indicate significant differences compared with the WT as determined by two-tailed Dunnett′s test (***P*<0.01).

(B) Representative images of WT (Col-0) and *syp61* constitutive knockdown mutant (*syp61 amiRNA*) seedlings grown for 8 days on 50 mM glucose/30 mM nitrogen, 150 mM glucose/0.3 mM nitrogen or 150 mM mannitol/0.3 mM nitrogen.

(C) Percentage of seedlings with green cotyledons after growth for 8 days. Glc, glucose; N, nitrogen; Man, mannitol; unit, mM. WT, wild-type. Data are means ± s.e.m. (n = 3 independent batches of plants). Statistical significance was determined by two-tailed Dunnett's test. (**P*<0.05, ***P*<0.01). n.s., not significant.

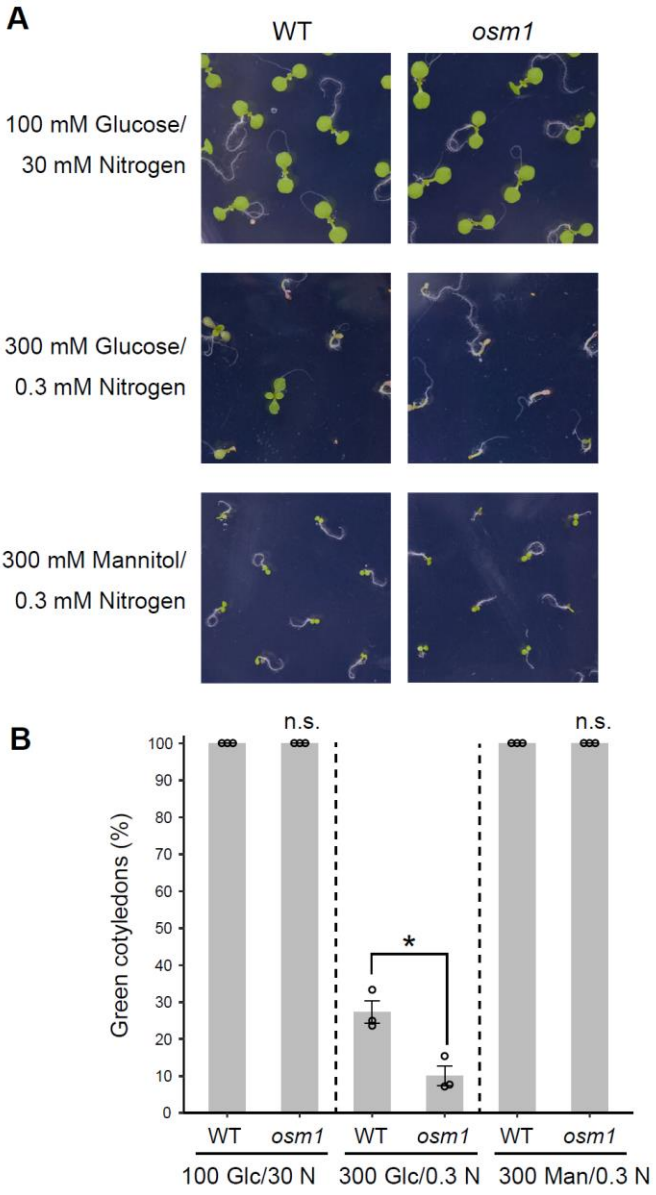
A
WT
osm1
100 mM Glucose/
30 mM Nitrogen
300 mM Glucose/
0.3 mM Nitrogen
300 mM Mannitol/
0.3 mM Nitrogen
B
n.s.
n.s.
Green cotyledons (%)
100
90
80
70
60
50
40
30
20
10
0
*
WT
osm1
WT
osm1
WT
osm1
100 Glc/30 N
300 Glc/0.3 N
300 Man/0.3 N

Fig. 9

Fig. 9 The *osm1* mutant is hypersensitive to C/N-nutrient stress.

C/N-nutrient responses during post-germination growth. Seedlings were grown on medium containing the indicated concentrations of glucose, nitrogen and mannitol (osmotic control).

(A) Representative images of WT (C24) and *osm1* seedlings grown for 10 days on 100 mM glucose/30 mM nitrogen, or 14 days on 300 mM glucose/0.3 mM nitrogen or 300 mM mannitol/0.3 mM nitrogen.

(B) Percentage of seedlings with green cotyledons after growth for 14 days. Glc, glucose; N, nitrogen; Man, mannitol; unit, mM; WT, wild-type. Data are means ± s.e.m. (n = 3 independent batches of plants). Statistical significance was determined by two-tailed Welch's *t*-test. (*P<0.05).

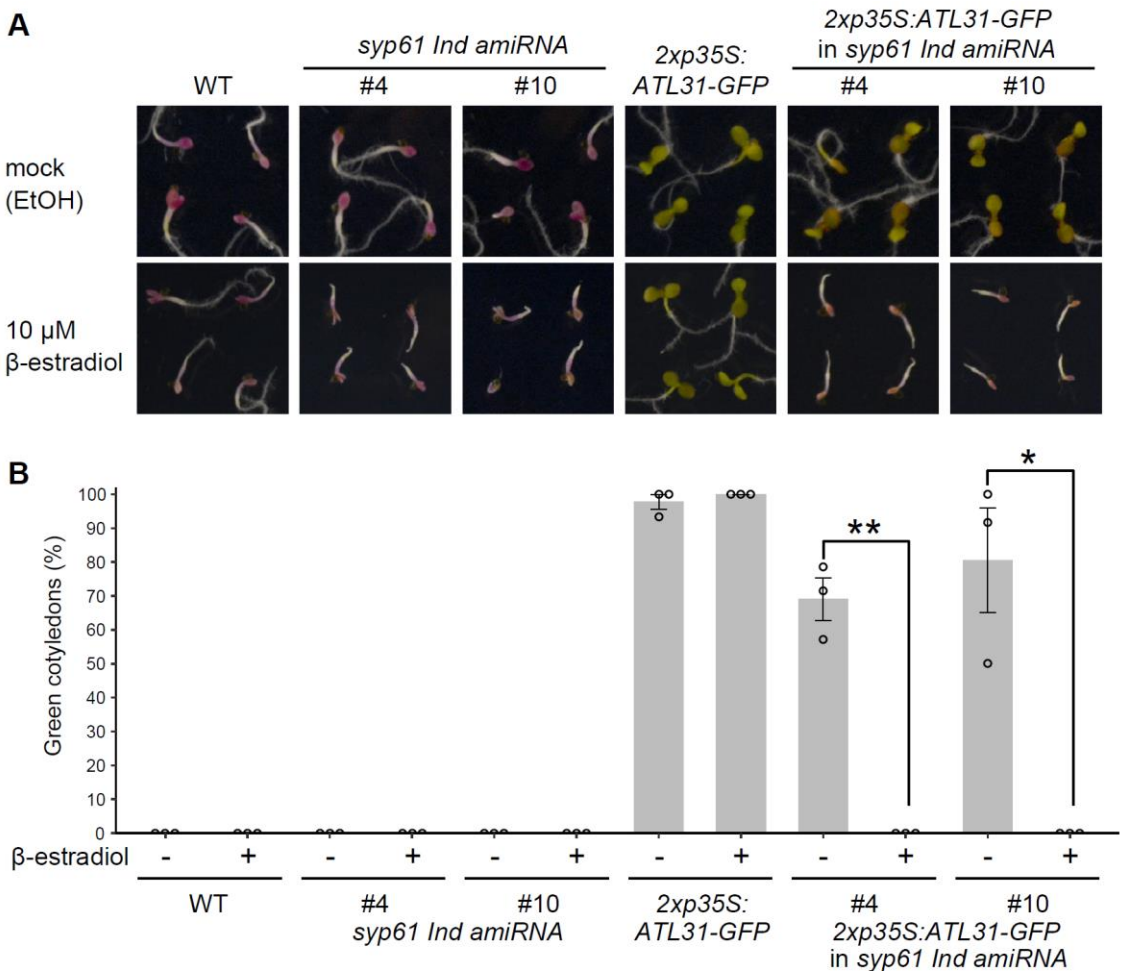
A
syp61 Ind amiRNA
2xp35S:ATL31-GFP in syp61 Ind amiRNA
WT
#4
#10
2xp35S: ATL31-GFP
#4
#10
mock (EtOH)
10 µM β-estradiol
B
Green cotyledons (%)
100
90
80
70
60
50
40
30
20
10
0
**
*
β-estradiol
- + - + - + - + - + - +
WT
#4 syp61 Ind amiRNA
#10
2xp35S: ATL31-GFP
#4 2xp35S:ATL31-GFP in syp61 Ind amiRNA
#10

Fig. 10

Fig. 10 Overexpression of *ATL31* did not rescue the C/N-nutrient stress hypersensitive phenotype of *SYP61* knockdown mutants.

(A) Representative images of WT (Col-0), *ATL31* overexpressor (*2xp35S:ATL31-GFP*), *syp61* inducible knockdown mutant (*syp61 Ind amiRNA*) and the F1 generation of the crossed plants grown for 12 days on 300 mM glucose/0.3 mM nitrogen with ethanol or β-estradiol.

(B) Percentage of seedlings with green cotyledons after growth for 12 days on 300 mM glucose/0.3 mM nitrogen with ethanol (-) or 10 μM β-estradiol (+). WT, wild-type. Data are means ± s.e.m. (n = 3 independent batches of plants). Statistical significance was determined by two-tailed Welch's *t*-test. (**P*<0.05, ***P*<0.01).

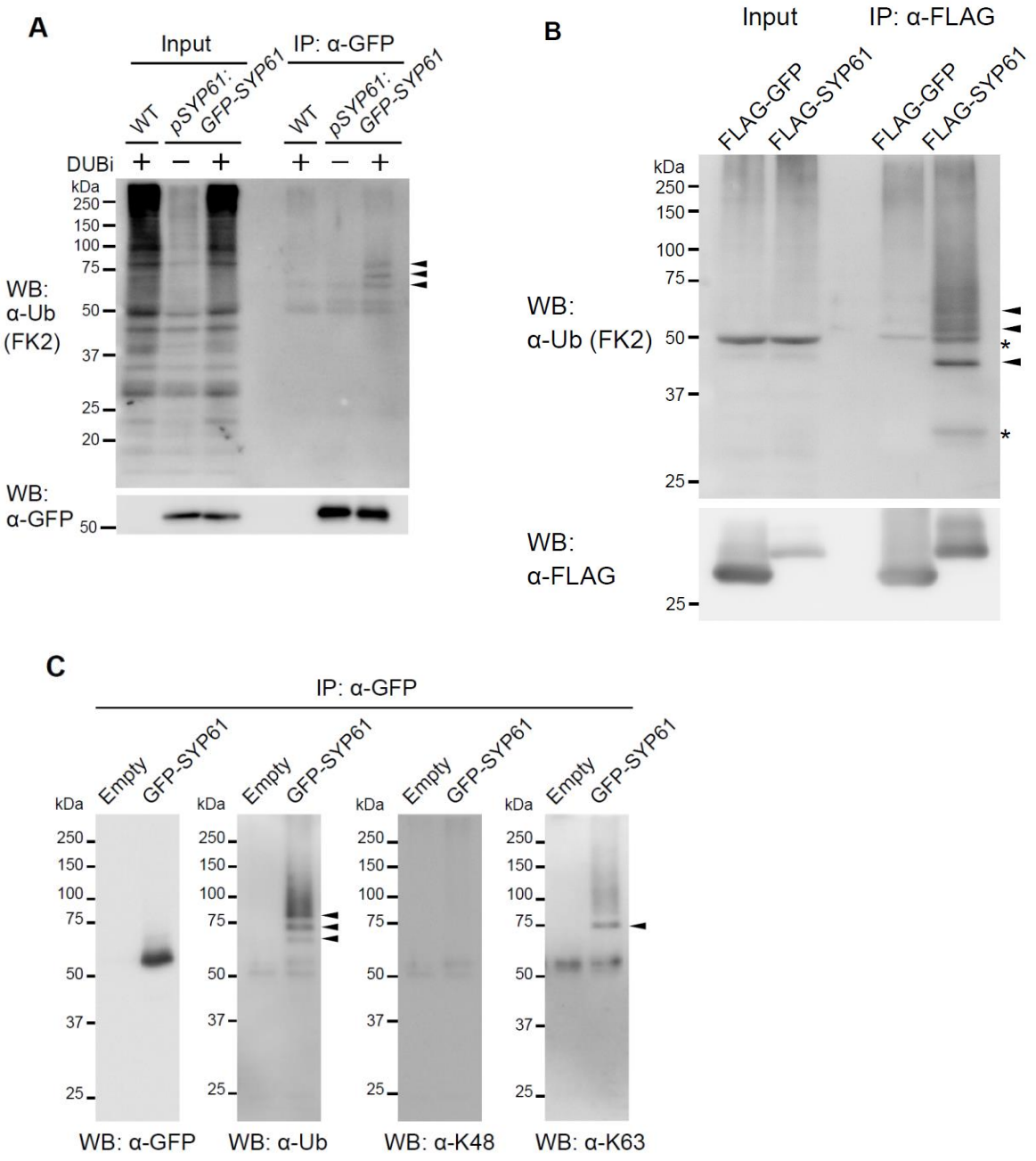
A
Input
IP: α-GFP
WT
pSYP61: GFP-SYP61
WT
pSYP61: GFP-SYP61
DUBi + − + + − +
kDa
250
150
100
75
50
37
25
20
WB: α-Ub (FK2)
WB: α-GFP
50
B
Input
IP: α-FLAG
FLAG-GFP
FLAG-SYP61
FLAG-GFP
FLAG-SYP61
kDa
250
150
100
75
50
37
25
WB: α-Ub (FK2)
WB: α-FLAG
25
C
IP: α-GFP
Empty
GFP-SYP61
Empty
GFP-SYP61
Empty
GFP-SYP61
Empty
GFP-SYP61
kDa
250
150
100
75
50
37
25
WB: α-GFP
WB: α-Ub
WB: α-K48
WB: α-K63

Fig. 11

Fig. 11 SYP61 is ubiquitinated in plants.

(A) Proteins were extracted from wild-type (WT) or GFP-SYP61 (55 kDa) expressing Arabidopsis plants (*pSYP61:GFP-SYP61*) in the presence or absence of deubiquitination enzyme inhibitors (DUBi). Proteins were immunoprecipitated with anti-GFP antibody beads, and detected by anti-ubiquitin (FK2) or anti-GFP antibodies. Arrowheads indicate ubiquitinated GFP-SYP61.

(B) FLAG-GFP (30 kDa) or FLAG-SYP61 (30.7 kDa) was transiently expressed in *N. benthamiana* leaves. Extracted proteins were immunoprecipitated with anti-FLAG antibody beads, and detected with anti-FLAG and anti-ubiquitin (FK2) antibodies. The FLAG-SYP61 bands were detected at higher position than expected. Arrowheads indicate ubiquitinated SYP61, and asterisks indicate unknown bands.

(C) GFP-SYP61 (56 kDa) was transiently expressed in *N. benthamiana* leaves. Extracted proteins were immunoprecipitated with anti-GFP antibody beads, and detected with anti-GFP, anti-ubiquitin (FK2), anti-K48-linked ubiquitin (Apu2), and anti-K63-linked ubiquitin (Apu3) antibodies. Arrowheads indicate ubiquitinated GFP-SYP61. The molecular weight of GFP-SYP61 for transient expression in *N. benthamiana* is higher than that of GFP-SYP61 in Arabidopsis stable plant, as it contains longer linker.

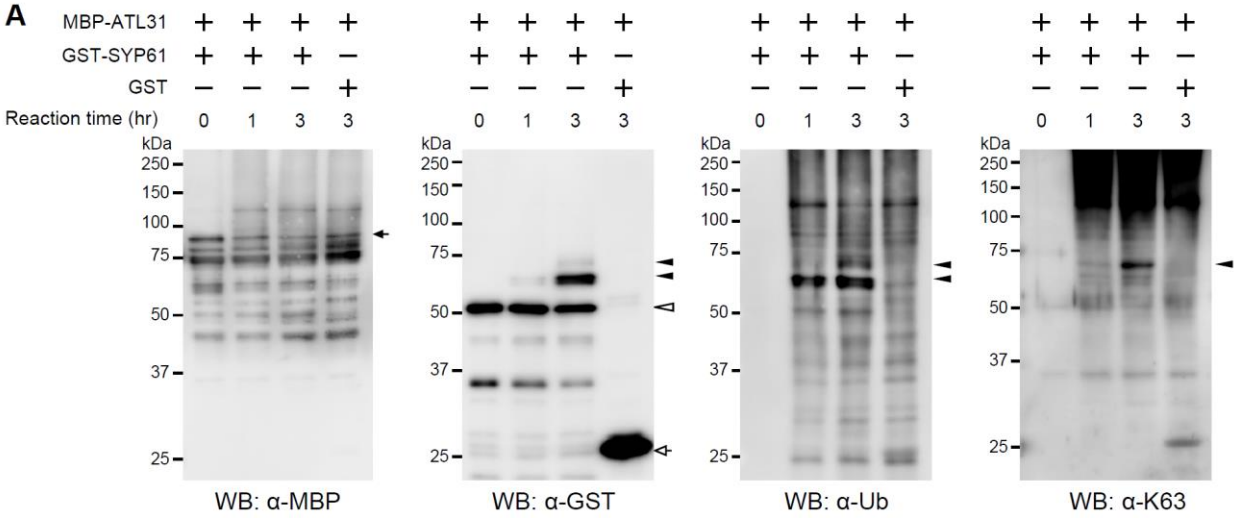
A
MBP-ATL31
GST-SYP61
GST
Reaction time (hr)
0 1 3 3
kDa
250
150
100
75
50
37
25
WB: α-MBP
WB: α-GST
WB: α-Ub
WB: α-K63

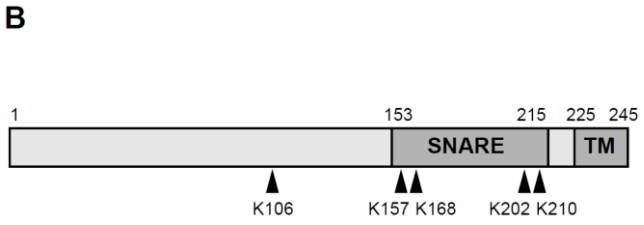
B
1
153
215
225
245
SNARE
TM
K106
K157 K168
K202 K210

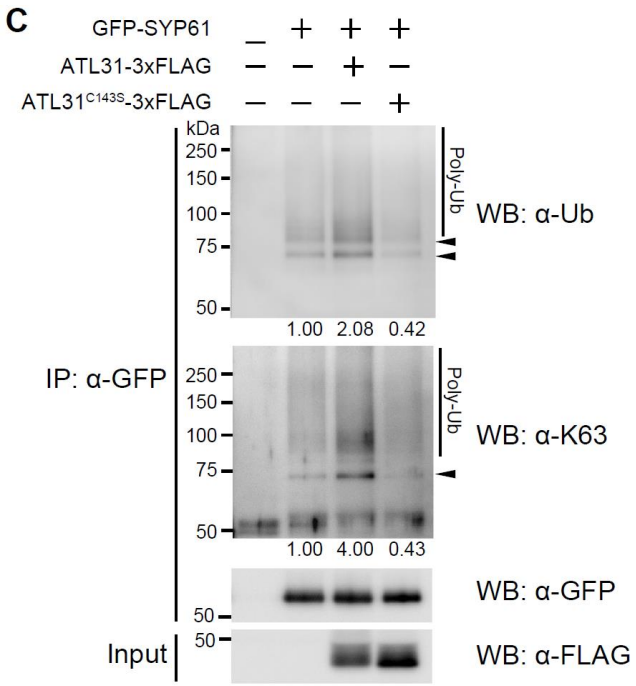
C
GFP-SYP61
ATL31-3xFLAG
ATL31C143S-3xFLAG
kDa
250
150
100
75
50
Poly-Ub
WB: α-Ub
1.00 2.08 0.42
IP: α-GFP
WB: α-K63
1.00 4.00 0.43
WB: α-GFP
Input
WB: α-FLAG

Fig. 12

Fig. 12 ATL31 ubiquitinates SYP61 *in vitro* and *in planta.*

(A) *In vitro* ubiquitination assay of SYP61 by ATL31. GST-SYP61 or GST was incubated with MBP-ATL31 in the presence of ubiquitin, E1, E2 and ATP for the indicated time. Immunoblot was performed with anti-MBP, anti-GST, anti-ubiquitin (FK2) and anti-K63-linked ubiquitin (Apu3) antibodies. Closed arrow, MBP-ATL31 (81 kDa); open arrow, GST (28 kDa); open arrowhead, GST-SYP61 (53 kDa); closed arrowheads, ubiquitinated SYP61.

(B) Schematic diagram of the primary structure of SYP61 protein. Arrowheads indicate the ATL31-catalyzed ubiquitination sites of SYP61, as determined by mass spectrometry analysis following *in vitro* ubiquitination assay as in **A**. Numbers are showing the amino acid positions. SNARE, SNARE domain; TM, transmembrane domain. The original data is shown in Supplemental Table 3.

(C) GFP-SYP61 (56 kDa) was transiently expressed alone or with ATL31-3xFLAG or ATL31$_{C143S}$-3xFLAG (45 kDa) in *N. benthamiana* leaves. Extracted proteins were immunoprecipitated with anti-GFP antibody beads, and detected with anti-GFP, anti-ubiquitin (FK2), and anti-K63-linked ubiquitin (Apu3) antibodies. Arrowheads indicate ubiquitinated GFP-SYP61. The numbers are showing the relative intensity of the di-Ub bands (the lower bands indicated in anti-ubiquitin) normalized by the band intensity of GFP-SYP61.

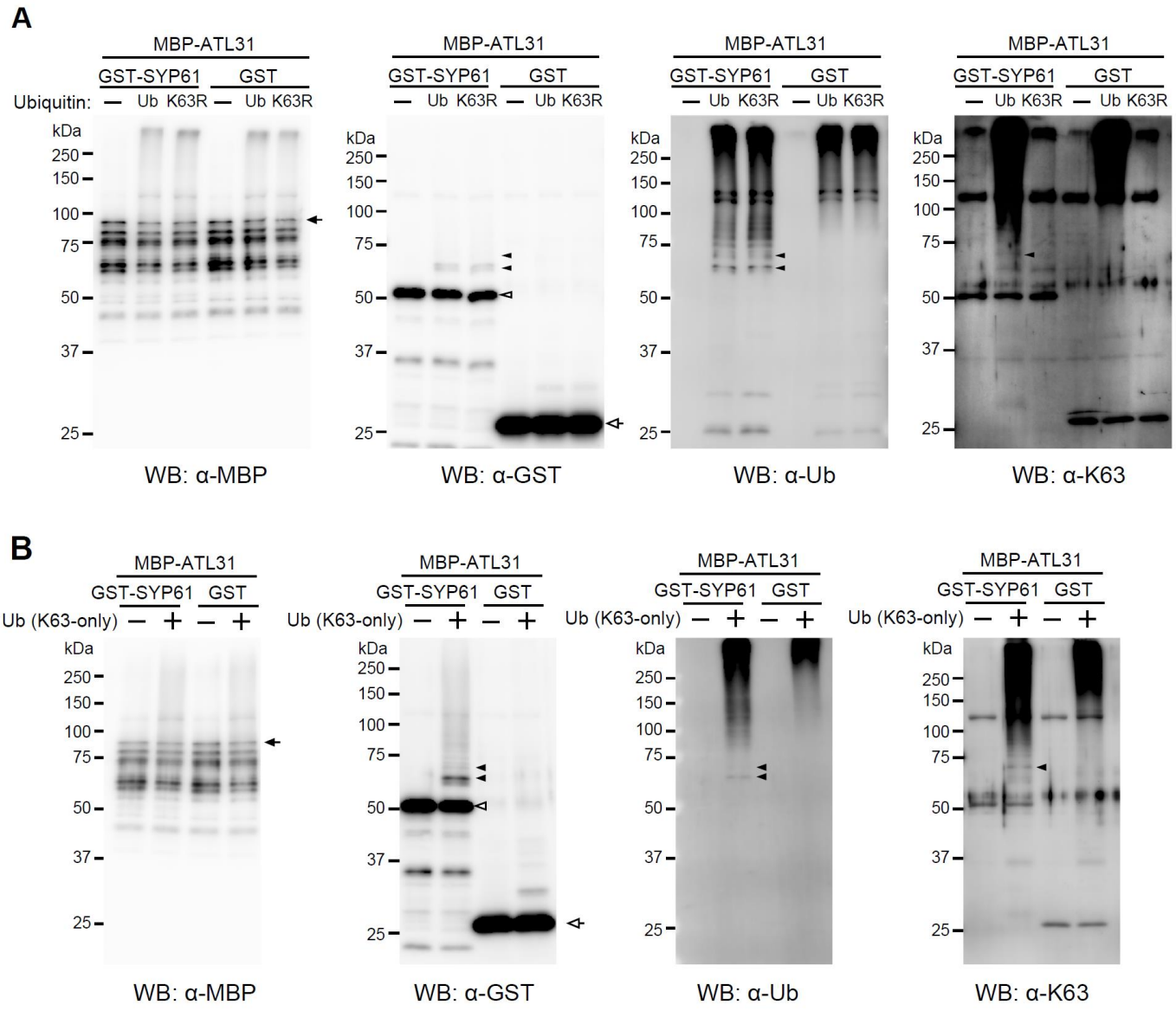
A
MBP-ATL31
GST-SYP61
GST
Ubiquitin:
—
Ub
K63R
—
Ub
K63R
kDa
250
150
100
75
50
37
25
WB: α-MBP
WB: α-GST
WB: α-Ub
WB: α-K63
B
Ub (K63-only)
WB: α-MBP
WB: α-GST
WB: α-Ub
WB: α-K63

Fig. 13

Fig. 13 ATL31 ubiquitinates SYP61 *in vitro.*

(A, B) *In vitro* ubiquitination assay of SYP61 by ATL31. GST-SYP61 or GST was incubated with MBP-ATL31 for 1 hour in the presence of E1, E2 and ATP, with or without indicated ubiquitin mutants: native ubiquitin (Ub) or K63R ubiquitin for **A**, and K63-only ubiquitin for **B**. Immunoblotting was performed with anti-MBP, anti-GST, anti-ubiquitin (FK2) and anti-K63-linked ubiquitin (Apu3) antibodies. Closed arrows, MBP-ATL31 (81 kDa); open arrows, GST (28 kDa); open arrowheads, GST-SYP61 (53 kDa); closed arrowheads, ubiquitinated SYP61.

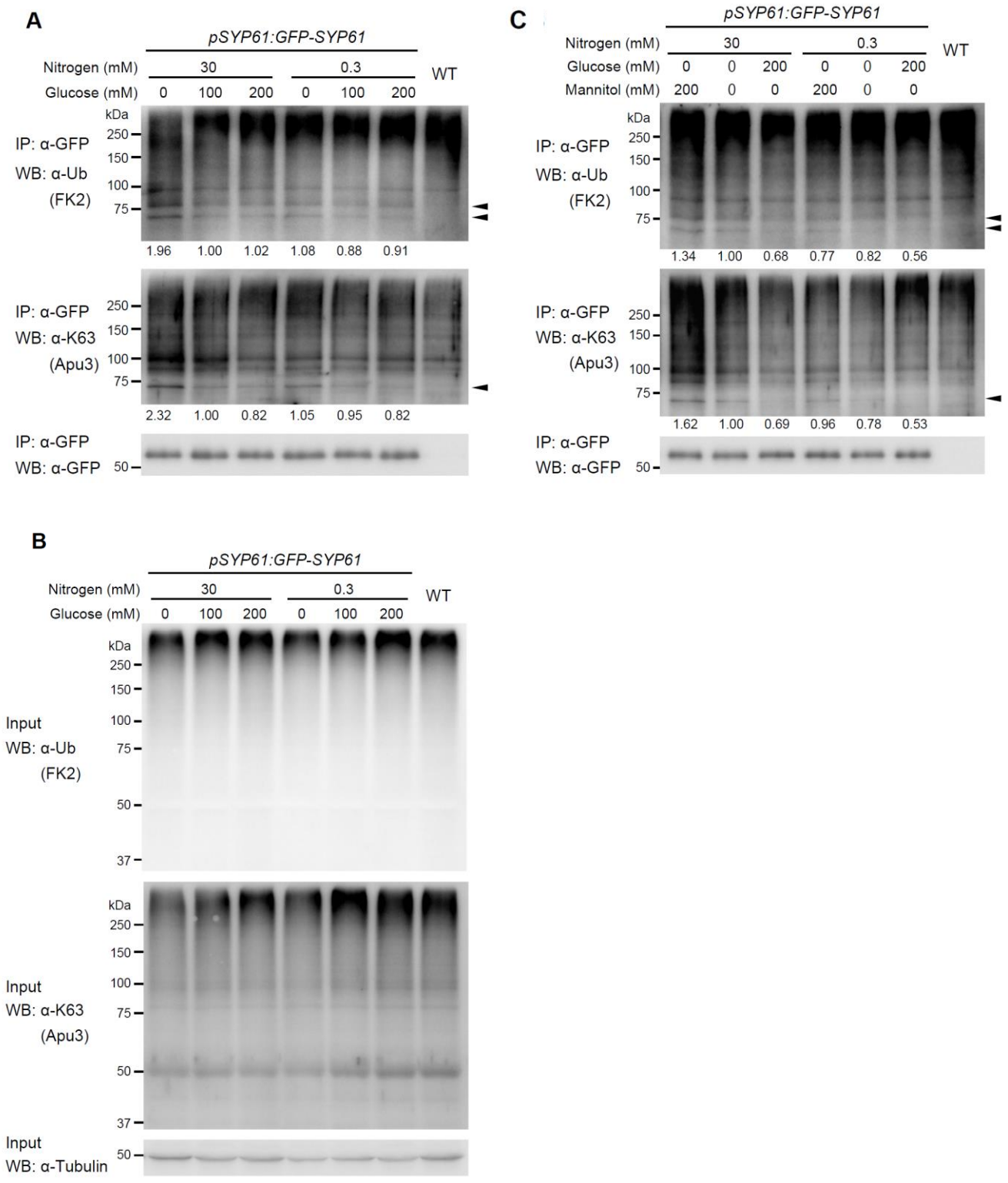
A
pSYP61:GFP-SYP61
Nitrogen (mM)
30
0.3
WT
Glucose (mM)
0 100 200 0 100 200
kDa
IP: α-GFP
WB: α-Ub
(FK2)
250
150
100
75
1.96 1.00 1.02 1.08 0.88 0.91
IP: α-GFP
WB: α-K63
(Apu3)
2.32 1.00 0.82 1.05 0.95 0.82
IP: α-GFP
WB: α-GFP
50
C
pSYP61:GFP-SYP61
Nitrogen (mM)
30
0.3
WT
Glucose (mM)
0 0 200 0 0 200
Mannitol (mM)
200 0 0 200 0 0
1.34 1.00 0.68 0.77 0.82 0.56
1.62 1.00 0.69 0.96 0.78 0.53
B
pSYP61:GFP-SYP61
Nitrogen (mM)
30
0.3
WT
Glucose (mM)
0 100 200 0 100 200
Input
WB: α-Ub
(FK2)
Input
WB: α-K63
(Apu3)
Input
WB: α-Tubulin
37
50

Fig. 14

Fig. 14 Ubiquitination of SYP61 is affected by C/N-nutrient availability.

GFP-SYP61 (55 kDa) expressing Arabidopsis plants (*pSYP61:GFP-SYP61*) were grown for 10 days in 100 mM glucose/30 mM nitrogen containing liquid medium, and treated with the medium containing indicated concentration of nitrogen and glucose **(A, B)**, or nitrogen, glucose and mannitol **(C)** for 3 hours. Extracted proteins were immunoprecipitated with anti-GFP antibody beads, and detected with anti-GFP, anti-ubiquitin (FK2), and anti-K63-linked ubiquitin (Apu3) antibodies (**A, C**). Input samples of the immunoprecipitation in **A** were detected with anti-ubiquitin (FK2) and anti-K63-linked ubiquitin (Apu3) antibodies (**B**). Arrowheads indicate ubiquitinated GFP-SYP61. The numbers are showing the relative intensity of the di-Ub bands (the lower band indicated in anti-ubiquitin) normalized by the band intensity of GFP-SYP61. WT, wild-type.

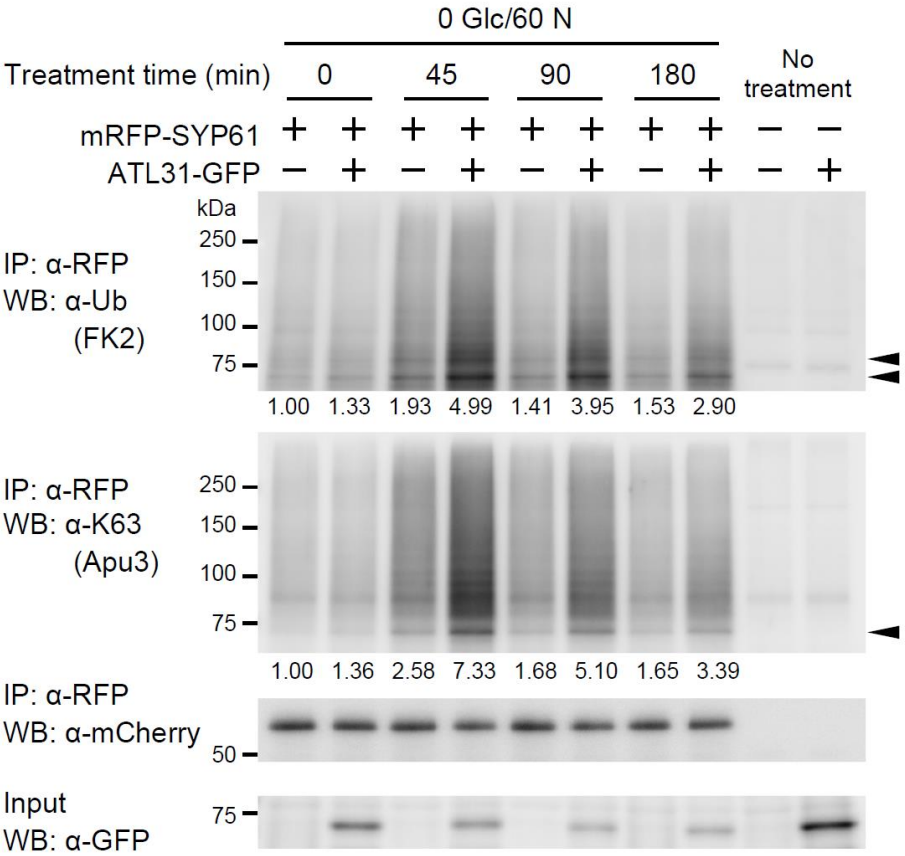
0 Glc/60 N
Treatment time (min)
0
45
90
180
No treatment
mRFP-SYP61
ATL31-GFP
kDa
IP: α-RFP
WB: α-Ub
(FK2)
250
150
100
75
1.00 1.33 1.93 4.99 1.41 3.95 1.53 2.90
IP: α-RFP
WB: α-K63
(Apu3)
250
150
100
75
1.00 1.36 2.58 7.33 1.68 5.10 1.65 3.39
IP: α-RFP
WB: α-mCherry
50
Input
WB: α-GFP
75

Fig. 15

Fig. 15 Low C/high N-nutrient responsive ubiquitination of SYP61 is enhanced by overexpression of ATL31.

Arabidopsis plants expressing mRFP-SYP61 (53 kDa) (*pSYP61:mRFP-SYP61*) in wild-type or ATL31-GFP overexpressor background (*2xp35S:ATL31-GFP*) were grown for 11 days in 100 mM glucose/30 mM nitrogen containing liquid medium, and treated with the medium containing 0 mM glucose/60 mM nitrogen for the indicated time. Wild-type and *2xp35S:ATL31-GFP* plants were used as negative controls. Extracted proteins were immunoprecipitated with anti-RFP antibody beads, and detected with anti-mCherry, anti-ubiquitin (FK2), and anti-K63-linked ubiquitin (Apu3) antibodies. ATL31-GFP in the crude extract was detected with anti-GFP antibody. Arrowheads indicate ubiquitinated mRFP-SYP61. The numbers are showing the relative intensity of the di-Ub bands (the lower band indicated in anti-ubiquitin) normalized by the band intensity of mRFP-SYP61. Glc, glucose; N, nitrogen; unit, mM.

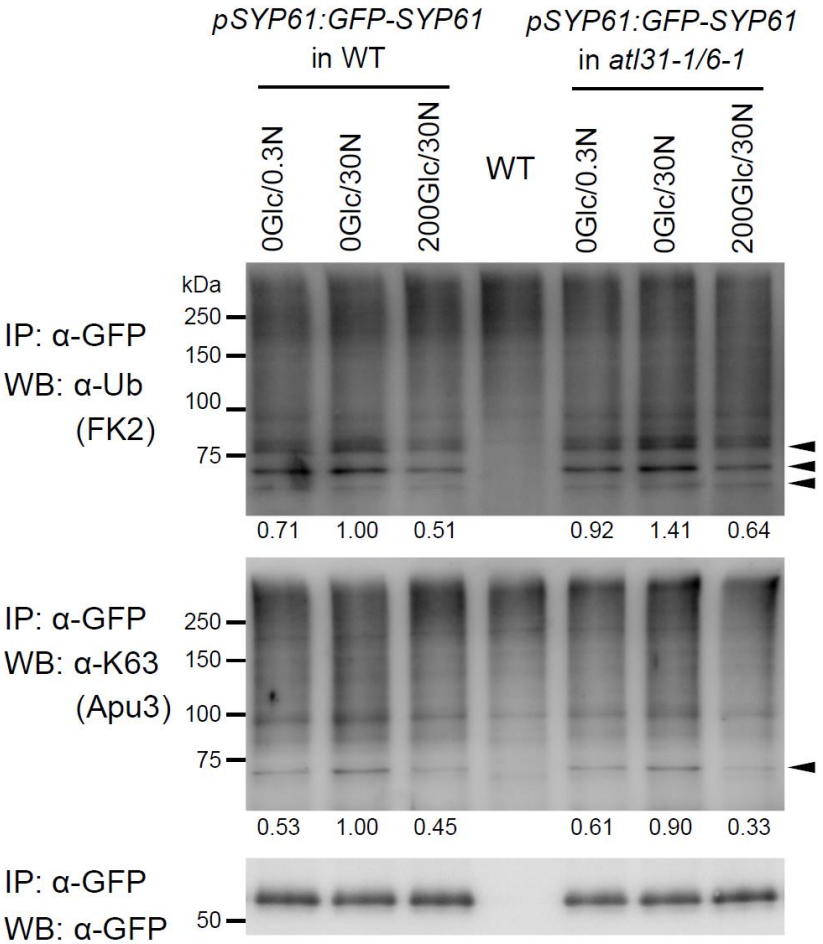
pSYP61:GFP-SYP61
in WT
pSYP61:GFP-SYP61
in atl31-1/6-1
0Glc/0.3N
0Glc/30N
200Glc/30N
WT
0Glc/0.3N
0Glc/30N
200Glc/30N
kDa
IP: α-GFP
WB: α-Ub
(FK2)
250
150
100
75
0.71
1.00
0.51
0.92
1.41
0.64
IP: α-GFP
WB: α-K63
(Apu3)
250
150
100
75
0.53
1.00
0.45
0.61
0.90
0.33
IP: α-GFP
WB: α-GFP
50

Fig. 16

Fig. 16 Ubiquitination of SYP61 in *atl31/6* double knockout mutant.

Arabidopsis plants expressing GFP-SYP61 (55 kDa) (*pSYP61:GFP-SYP61*) in wild-type or *atl31-1/6-1* double knockout mutant background (F5 generation, homo) were grown for 10 days in 100 mM glucose/30 mM nitrogen containing liquid medium, and treated with the medium containing indicated concentration of glucose and nitrogen for 3 hours. Extracted proteins were immunoprecipitated with anti-GFP antibody beads, and detected with anti-GFP, anti-ubiquitin (FK2), and anti-K63-linked ubiquitin (Apu3) antibodies. Arrowheads indicate ubiquitinated GFP-SYP61. The numbers are showing the relative intensity of the di-Ub bands (the middle band indicated in anti-ubiquitin blot) normalized by the band intensity of GFP-SYP61. Glc, glucose; N, nitrogen; unit, mM. WT, wild-type.

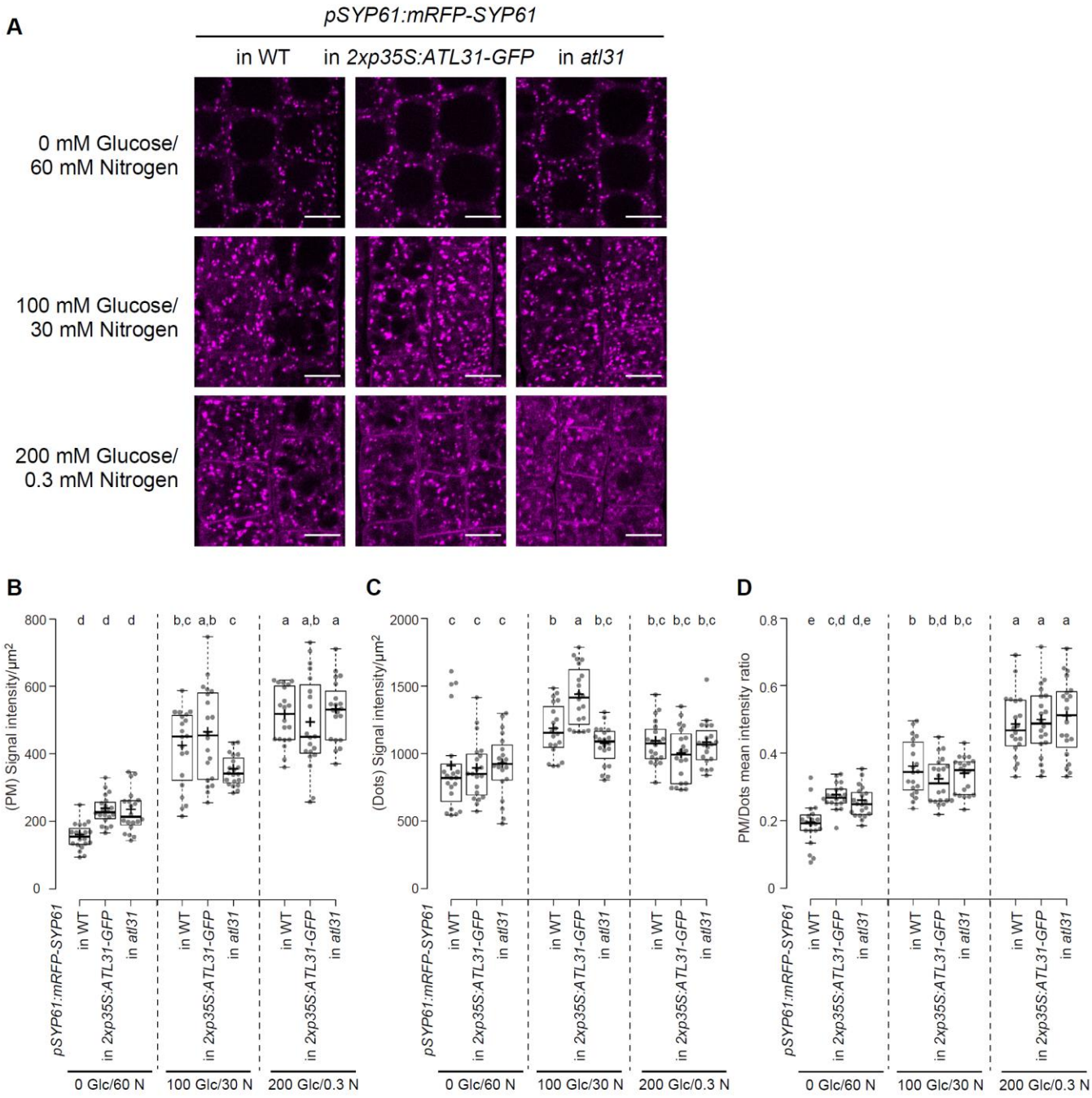
A
pSYP61:mRFP-SYP61
in WT
in 2xp35S:ATL31-GFP
in atl31
0 mM Glucose/
60 mM Nitrogen
100 mM Glucose/
30 mM Nitrogen
200 mM Glucose/
0.3 mM Nitrogen
B
(PM) Signal intensity/µm²
C
(Dots) Signal intensity/µm²
D
PM/Dots mean intensity ratio
pSYP61:mRFP-SYP61
in WT
in 2xp35S:ATL31-GFP
in atl31
0 Glc/60 N
100 Glc/30 N
200 Glc/0.3 N

Fig. 17

Fig. 17 The plasma membrane localization of SYP61 in response to C/N-nutrient conditions in different genotype background.

(A) Representative confocal images of Arabidopsis root epidermal cells expressing mRFP-SYP61 in wild-type (WT), ATL31 overexpressor (*2xp35S:ATL31-GFP*), or *atl31-1* knockout mutant. Plants were treated with liquid MS medium containing 0 mM glucose/60 mM nitrogen, 100 mM glucose/30 mM nitrogen or 200 mM glucose/0.3 mM nitrogen overnight, and the 6 day-old plants were observed. Bars = 10 μm

(B, C) Mean signal intensity of the mRFP-SYP61 in the plasma membrane (B) or the dot-like structures (C).

(D) Signal intensity ratio of the plasma membrane to the dot-like structures.

(B, C, D) Box plots definition: center line, median; box limits, lower and upper quartiles; dots, individual data points; whiskers, highest and lowest data points (The whiskers extend to data points that are less than 1.5 x IQR away from 1st/3rd quartile). n = 20 cell slices from 5 roots were analyzed. Statistical differences were inferred by analysis of variance (ANOVA) followed by Tukey´s honestly significant difference (HSD) test. Different letters are indicating significant difference ($P<0.05$).

TABLES OF SUPPORTING INFORMATION

Supplemental Table 1. Primer sequences used for the plasmid construction.

Gene	Sequence (Forward, 5'→3')	Sequence (Reverse, 5'→3')
SYP61	CACCATGTCTTCAGCTCAAGA	GGTCAAGAAGACAAGAACGAA
UBQ1	CACCATGCAGATCTTCGTGAAA	CTAACCTCCTCTAAGCCTCAACAC
ATL31-3xFLAG	CACCATGGATCCCATAAAACACAT	CTAAGATCTCTTGTCATCGTCATC

Supplemental Table 2. Primer sequences used for expression analysis.

Gene	Sequence (Forward, 5'→3')	Sequence (Reverse, 5'→3')
SYP61	GATTCAGGATTCTATTGATAAGTTGC	CTCATCTACCTGCCACTCAATG
ATL31	ACCGGTGGGCTTTTCTTAG	AACTGACGATGTTCCTTCACC
18S rRNA	CGGCTACCACATCCAAGGAA	GCTGGAATTACCGCGGCT

Supplemental Table 3.

Ubiquitinated SYP61 peptides detected by mass spectrometry analysis.

Peptide sequence[a]	Position	q-Value[b]	XCorr[b]
SGVLAG**K**VSSGAGHASEVR	K106	0	3.21
QMLLI**K**QQDEELDELSK	K157	0	1.94
QQDEELDELS**K**SVQR	K168	0	2.39
IIDELDTEMDST**K**NR	K202	0	3.50
IIDELDTEMDST**K**NRLEFVQK	K202	0	2.45
NRLEFVQ**K**K	K210	0	2.76

[a]Ubiquitinated lysine (K) residue is indicated by bold letter with underline.
[b]The scores assigned by SEQUEST software after database searching.

CONCLUSION

In this study, I aimed to clarify the functional interaction of the ubiquitin ligase ATL31 and its novel interactor SYP61, the crucial SNARE protein that mediates post-*Golgi* membrane trafficking in Arabidopsis. Using molecular biological approaches including biochemical, physiological, and cell biological analyses, I demonstrated that SYP61 is necessary for the high C/low N-nutrient stress tolerance mediated by ATL31, while ATL31 has an ability to ubiquitinate SYP61, which is transiently enhanced in low C/high N-nutrient conditions. While the ubiquitination of SYP61 by ATL31 in plants needs further confirmation, this research clearly illustrated the effect of nutrient conditions on the SNARE ubiquitination, as well as the critical role of a SNARE protein in plant nutrient responses.

Several recent reports showed ubiquitination-mediated regulations of SNARE proteins in yeast and mammals. This research implicated ubiquitination in SNARE protein regulations also in plants. This study also showed the SNARE ubiquitination that responds to nutrient conditions in any organism. Further research should reveal the downstream effect of this post-translational modification. Through the elucidation of the molecular interactions between ATL31 and SYP61, this research widened our view of the ubiquitin signaling and membrane trafficking machinery in plant nutrient responses.

PUBLICATION LIST

1. **Yoko Hasegawa,** Thais Huarancca Reyes, Tomohiro Uemura, Anirban Baral, Akari Fujimaki, Yongming Luo, Yoshie Morita, Yasushi Saeki, Shugo Maekawa, Shigetaka Yasuda, Koki Mukuta, Yoichiro Fukao, Keiji Tanaka, Akihiko Nakano, Junpei Takagi, Rishikesh P. Bhalerao, Junji Yamaguchi and Takeo Sato. (2022) The TGN/EE SNARE protein SYP61 and the ubiquitin ligase ATL31 cooperatively regulate plant responses to carbon/nitrogen conditions in Arabidopsis. ***The Plant Cell***, Oxford University Press, https://doi.org/10.1093/plcell/koac014

PUBLICATION LIST (APPENDIX)

1. Yongming Luo, Junpei Takagi, Lucas Claus, Chao Zhang, Shigetaka Yasuda, **Yoko Hasegawa**, Junji Yamaguchi, Libo Shan, Eugenia Russinova, and Takeo Sato (2022) Deubiquitinating enzymes UBP12 and UBP13 stabilize the brassinosteroid receptor BRI1. ***EMBO Reports***, Wiley-VCH, https://doi.org/10.15252/embr.202153354

2. Shoki Aoyama, Saki Terada, Miho Sanagi, **Yoko Hasegawa**, Yu Lu, Yoshie Morita, Yukako Chiba, Takeo Sato, Junji Yamaguchi (2017) Membrane-localized ubiquitin ligase ATL15 functions in sugar- responsive growth regulation in Arabidopsis. ***Biochemical and Biophysical Research Communications***, ELSEVIER, 491, pp33-39

3. Shigetaka Yasuda, Shoki Aoyama, **Yoko Hasegawa**, Takeo Sato, and Junji Yamaguchi (2017) Arabidopsis CBL-Interacting Protein Kinases Regulate Carbon/Nitrogen-Nutrient Response by Phosphorylating Ubiquitin Ligase ATL31. ***Molecular Plant***, Cell press, 10, pp605–618

4. Xingwen Li, **Yoko Hasegawa**, Yu Lu and Takeo Sato (2017) Ubiquitin related enzymes and plant-specific ubiquitin ligase ATL family in tomato plants. ***Plant Biotechnology***, J-STAGE, 34, pp71-78 (Review paper)